Final Report

Comparative Modeling Studies of Reservoir Drawdown Induced Erosion and Sedimentation

Agreement Numbers: R12AC80424

Principal Investigator:
Jennifer G. Duan, Ph.D., PE, Associate Professor
Department of Civil Engineering and Engineering Mechanics.
University of Arizona

Researchers:
Chunshui Yu, Post-doc Research Associate
Department of Civil Engineering and Engineering Mechanics
University of Arizona

Asadi Khalid, PhD Candidate
Department of Civil Engineering and Engineering Mechanics
University of Arizona

Liu Lei, PhD Candidate, Visiting Student
Department of Civil Engineering and Engineering Mechanics
University of Arizona

Sept 19th, 2014

Executive Summary

This report summarizes the verification of SRH2D model for simulating flow hydrodynamics and sediment transport in alluvial rivers. SRH2D model is a depth-averaged two-dimensional model for flow and sediment transport in alluvial rivers developed by the Bureau of Reclamation. In Part 1, the SRH2D model is verified by using two laboratory experiments: one is turbulent flow passing through a series of spur dikes, and the other is dam break flow over a mobile bed. The results showed that SRH2D model is capable of simulating turbulence flow field around dikes, and the simulated turbulence properties approximately matched the measurements. The model was also applied to simulate dam break flow over mobile bed, the simulated flow field and bed elevation changes matched the measurements very well.

In Part 2 and Part 3, SRH2D model is applied to simulate the fluvial processes during the 1994 Lake Mills drawdown experiment. The experimental drawdown was performed in April 1994 by gradually lowering the lake level by 18 feet over one week period. Flow discharge, cross sectional data, and sediment size distribution were collected at the reservoir reach during the experiment. This study simulated flow hydrodynamics and sediment transport during the experimental drawdown. The simulation used surveyed cross section data to reconstruct the lake bathymetry. Measured flow discharge and sediment load were used as the upstream boundary conditions for flow and sediment. Observed lake levels in the reservoir were the downstream boundary condition. Multiple simulation runs using different sediment transport formulas, computational meshes, and various Manning's roughness are compared with field surveyed data. Results showed the model underestimated erosion occurred during the drawdown experiment.

To verify SRH2D model, the Delft3D model is also used to simulate the drawdown experiment. Results of bed elevation changes using the Delft3D model are worse than those of SRH2D. Delft3D model predicted deposition rather than erosion during this drawdown experiment except at the edge of delta.

Based on the results from both models, two factors may attribute to the underestimation of erosion during the drawdown experiment. One factor is flow hydrodynamics, because no field data of flow field (velocity/flow depth) are available to verify the simulated hydrodynamic flow field. The other factor is the erosion due to vertically accelerating flow, which is caused by the rapid decreasing of surface elevation. The impact of this vertical flow on sediment transport was not considered in either model.

Part 1. Verification of SRH2D Model Using Laboratory Experiment

1.1 Flow Model Verification Using Flow Over Series of Spur Dikes

1.1.1 Introduction

This part summarizes the verification of SRH-2D model for simulating hydrodynamic flow field, especially turbulent kinetic energy (TKE), using an experiment of flow field around a series of spur dikes at the University of Arizona. SRH-2D, Sedimentation and River Hydraulics – Two Dimensional model, is two-dimensional hydraulic, sediment, temperature, and vegetation model for river systems developed at the Bureau of Reclamation. The spur dike experiment was conducted in a rectangular flume with a mobile bed surface having a well-sorted sand and gravel mixture. After the scoured bed reached the equilibrium state, bed sediments were immobilized with a thin layer of cement. The flow velocities, depths, and bed elevations over the scoured immobile bed surfaces were measured. This study simulated the hydrodynamics flow field using the scoured bed, and compared the simulated TKE with the measured ones. The SRH2D simulated results were also compared with the simulated results by using the FLOW3D software.

The spur dike experiment was conducted in a recirculating flume located at the Department of Civil and Engineering Mechanics, University of Arizona. The recirculating flume is 12.m long, 0.6 m wide, and 1.2 m deep. Three dikes of 30 cm length, 0.4 cm thickness and 40 cm height were protruded from the left-wall of the flume facing upstream at an angle of 150 degrees with a distance of 30 cm in between. The first angled dike was located at 1.8 m downstream of the flume inlet (Fig.1.1). The duration of the experimental run was 24 hours to allow the local scour reaches an asymptotic state. After the scoured bed reached the equilibrium state, bed surface was immobilized with a thin layer of cement. Then, the flow field (velocity and depth) and bed surface were measured (Fig.1.2).

Fig. 1.1 Picture of scoured bed surface
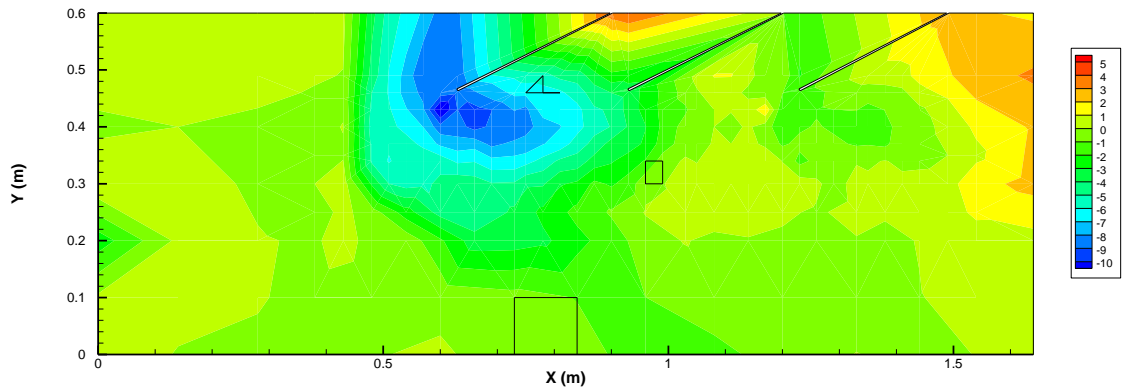
Fig. 1.2 Measured bed bathymetry (cm) of the developed scour hole

1.1.2 Computational Mesh

This study defines the x coordinate is in the streamwise direction, and the y-coordinate is in the cross stream direction. The origin of the coordinates were set at 0.63 m upstream of the tip of the first spur dike. The computational mesh was generated using SMS 10.1. Only the triangular element is used in this study. The mesh spacing is 5 cm (Fig.1.3).
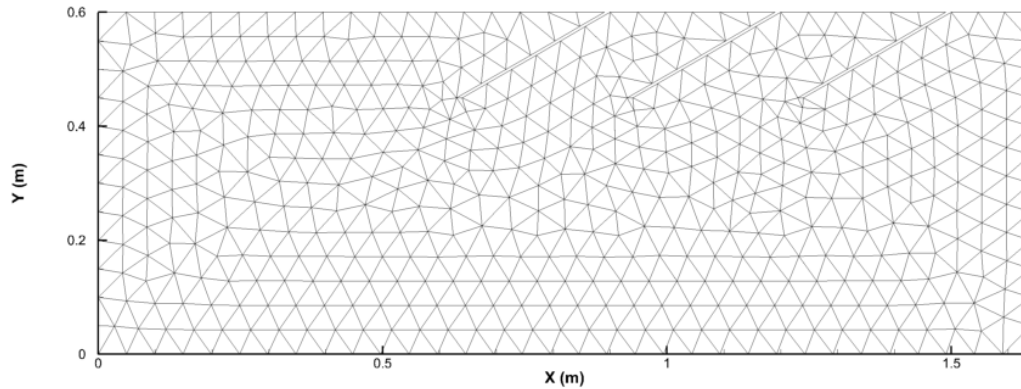
Fig.1.3 Computational mesh with 5cm spacing

1.1.3 Turbulence Model

The κ-ε turbulence closure model available in SRH2D model was chosen in the simulation.

1.1.4 Initial and Boundary Conditions

Since the simulation is a steady state solution, the "AUTO" type initial condition was selected. The total discharge boundary condition, Q = 0.035 m^3/s, is set at the inlet boundary. And the outlet boundary is the constant water surface elevation (h = 0.2 m). Bed bathymetry is the scoured bed surface.

1.1.5 Results

The experimental result of TKE distribution is shown in Fig.1.4. The SRH2D simulated results are shown in Fig.1.5, and Flow3D results are in Fig.1.6. The comparisons of all the measured TKE with the simulated ones are shown in Fig.1.7.

In general, neither SRH2D nor FlOW3D can predict the measured TKE, which is the maximum around the 1st dike where the scour hole was developed. The simulated TKE from FLOW3D model is slightly better than SRH2D model as shown in Fig.1.7.
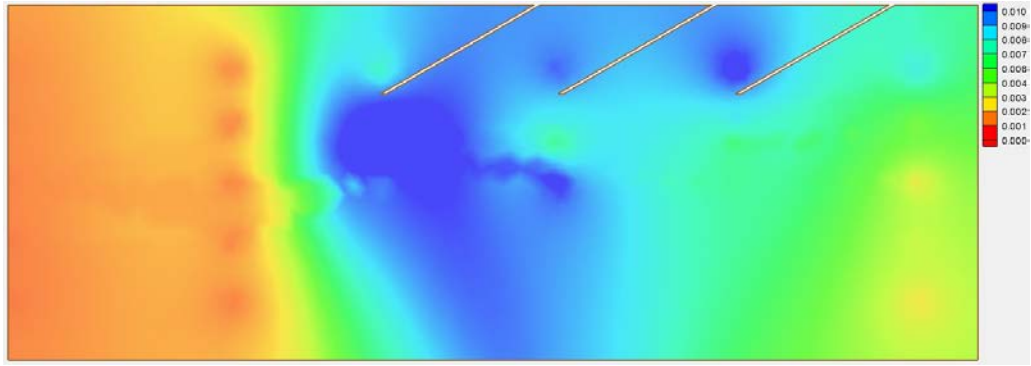
Fig.1.4 Measured TKE distribution around dikes
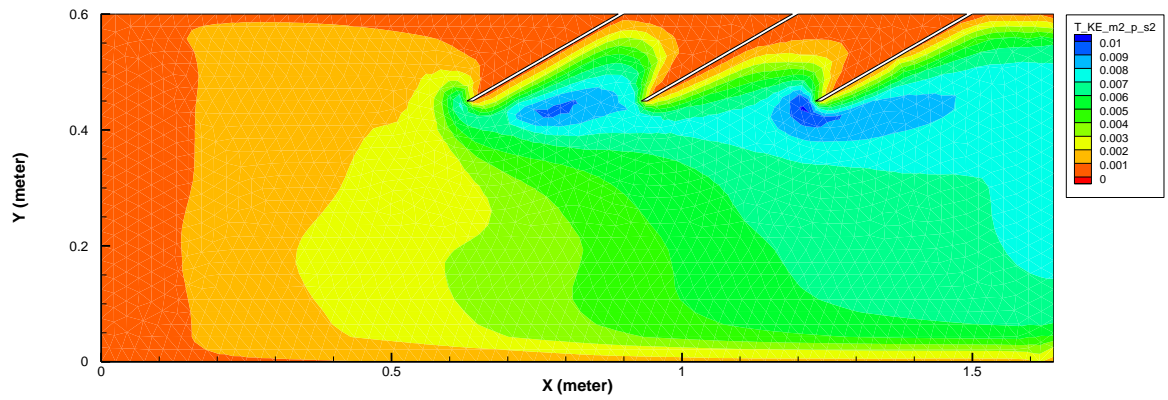
Fig.1.5 SRH2D simulated TKE distribution around dikes
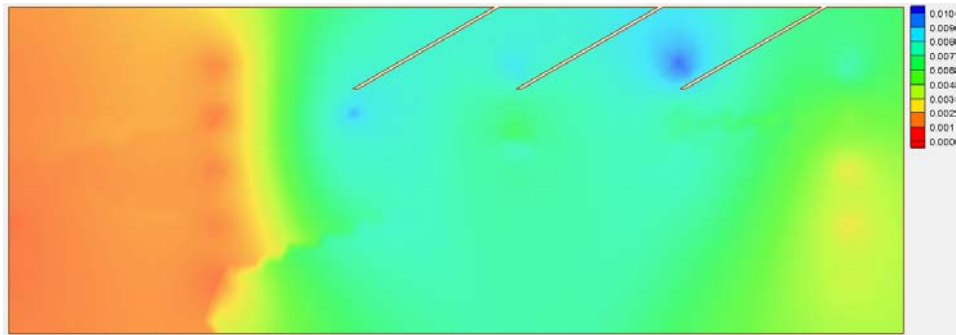
Fig.1.6 FLOW3D simulated TKE distribution around dikes
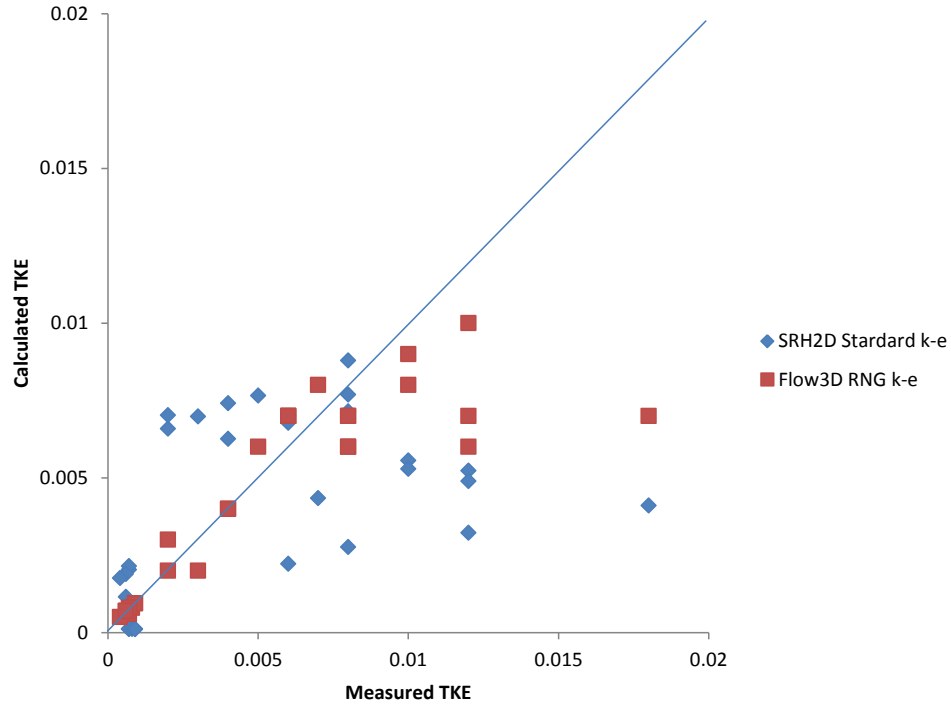
Fig.1.7 Comparison of measured, SRH2D and FLOW3D simulated TKE distribution around dikes

1.2 Verification of the Updated SRH2D Model for Bed Shear Stress Prediction

1.2.1 Bed Shear Stress for Sediment Transport

For non-uniform and unsteady flows in laboratory open channels or natural rivers, bed shear stress is important for estimating sediment transport rate. However, among many methods to calculate bed shear stresses in the literature, civil engineers often adopt the Reynolds stresses method in Dey and Barbhuiya (2005). If using the near-bed Reynolds stresses to approximate bed shear stress, τ_b, the mathematical equation is

$$\tau_b = \sqrt{\left(\tau_b^{\,x}\right)^2 + \left(\tau_b^{\,y}\right)^2} \tag{1.2.1}$$

where $\tau_b^{\,x} = -\rho\left(\overline{w'u'} + \overline{v'u'}\right)\Big|_{bed}$ and $\tau_b^{\,y} = -\rho\left(\overline{w'v'} + \overline{v'u'}\right)\Big|_{bed}$, in which $\tau_b^x, \tau_b^y =$ bed shear stresses in x and y directions, respectively; ρ =density of water, $u', v', w' =$ turbulence intensities in x, y and z directions, respectively. An alternate method to calculate bed shear stress uses only the Reynolds stresses relating to w' component, and the equation becomes:

10

$$\tau_b = -\rho(\overline{u'w'} + \overline{v'w'}) \tag{1.2.2}$$

When the turbulence intensity in the transverse direction is insignificant, a simple form is used instead of Eq. (1.2.2) (Biron 2005):

$$\tau_b = -\rho(\overline{u'w'}). \tag{1.2.3}$$

Another common method of calculating the bed shear stress involves the turbulent kinetic energy. This method uses the turbulent fluctuations in the three spatial directions, u', v', and w'.

$$\tau_b = C_1[\frac{1}{2}\rho(u'^2 + v'^2 + w'^2)] \tag{1.2.4}$$

where C_1 is a proportionality constant equal to 0.19 (Kim, *et al.*, 2000, Pope, *et al*, 2006). Because the instrument noise error associated with vertical velocity fluctuations is smaller than that associated with the horizontal fluctuations, bed shear stress can also be calculated using only w' as:

$$\tau_b = C_2\rho(w'^2) \tag{1.2.5}$$

where $C_2 = 0.9$. Among these five methods of calculating bed shear stress, we selected Eqs. (1.2.1), (1.2.2), (1.2.4) and (1.2.5) to calculate bed shear stress in a groin field to determine which one would give the most accurate results. The flume experiments were performed in 2008 at Univ. of Arizona (Fig.1.8). The measurement locations are shown in Fig.1.9. Turbulence flow field is measured using a 25 Hz micro-ADV.
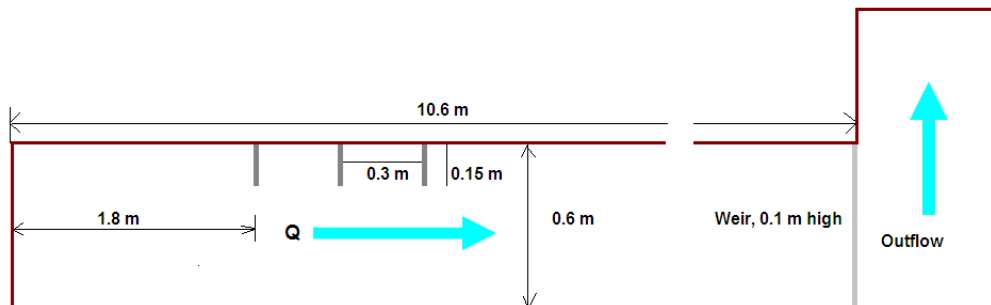
Fig.1.8 Plan view of the flume set up.
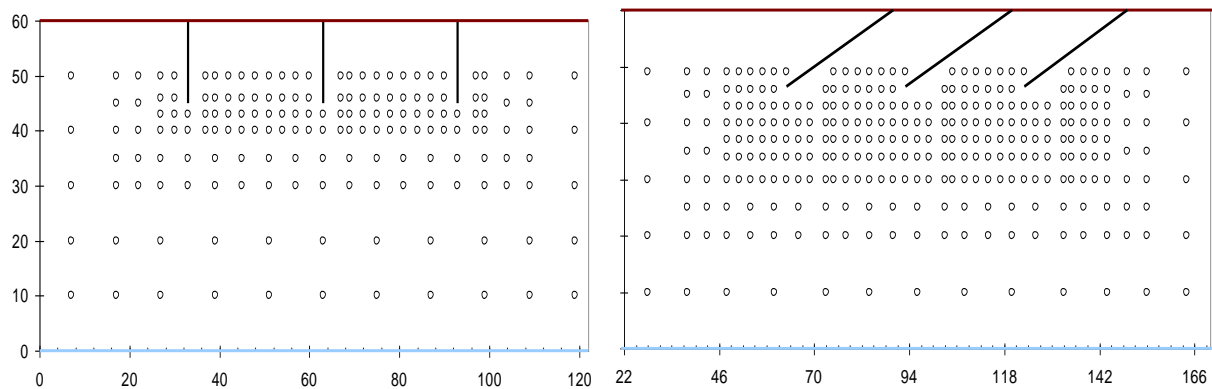
Fig.1.9 Measurement grid for the straight (*left*) and angled (*right*) dikes.

At first, the bed shear stress calculated by using the method in Dey and Barbhuiya (2005) was compared to the one calculated by using the TKE method as shown in Fig.1.10 (a). Dey's and Barbhuiya's method yielded a bed shear stress nearly $2 - 4$ times of those from the TKE method. As the Reynolds number increased, the correlation of bed shear stresses from these two methods became worse. Secondly, bed shear stresses obtained from only considering the Reynolds stresses associated with *w'* were also compared with the bed shear stresses from TKE method in Fig.1.10 (b). The Reynolds stress method that only considers the *w'* component yielded much smaller bed shear stresses than the TKE method. Because turbulent flow around the dikes is highly three-dimensional, this excludes the use of this method. Since accurate ADV measurements require the primary receiver pad to be aligned with the streamline, measurements collected around the dike apparently were not able to be aligned with the curved streamlines.

Many applications of ADVs in tidal flows (Kim, et al., 2000; Huthnance, 2002; Pope, et al, 2006; McLelland and Nicholas 2000; Biron et al 2004; McVicar and Roy 2007) concluded that the TKE method is the most reliable to estimate the bed shear stress. It is worthy to point out that Biron et al. (2004) compared these three methods for calculating bed shear stress and suggested that the method using *w'* is not appropriate for complex flow field around dikes. Therefore, this comparison suggested the TKE method for calculating bed shear stress.
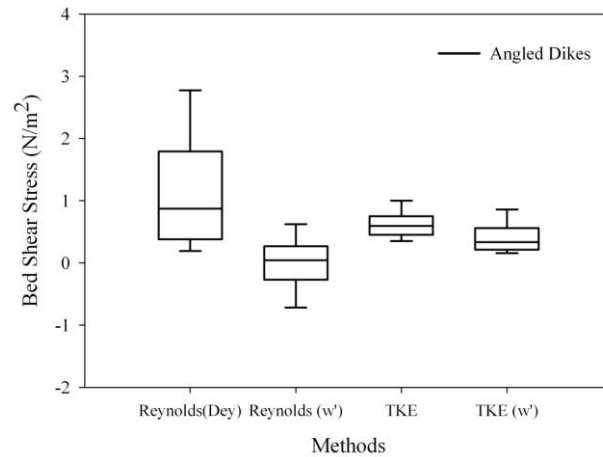
(a) Angled dikes on flat bed
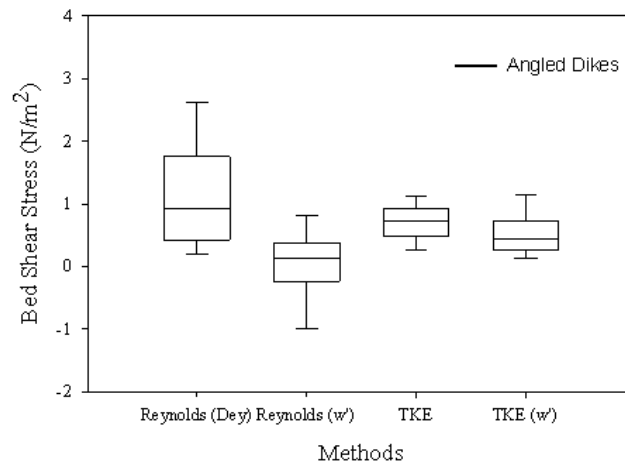
(b) Angled dikes on scoured bed

Fig.1.10 Comparison of different methods of calculating τ for straight and angled dikes.

1.2.2 Verification Case

Based on the conclusion from Section 1.2.1, the SRH2D model is updated by using the TKE to approximate the bed shear stress. The updated SRH2D is applied to re-simulate the flow field passing through the series of three dikes described in Section 1.1. This simulation is different from the one in Section 1.1, where the scoured bed surface is fixed. This simulation utilized the mobile bed function in SRH2D model that simulates the development of scour hole around the series of dikes. The following are descriptions of model set-ups and results.

1.2.2.1 Computational Mesh

The same 5 cm spacing triangular mesh is used in the simulation.

1.2.2.2 Turbulence Model

Both the parabolic and the κ-ε turbulence closure model were used in the tests. For the parabolic model, the default model constant (0.7) is used.

1.2.2.3 Sediment Transport Model

The mobile bed surface is 10 cm thickness of a well-sorted sand and gravel mixture. The median grain diameter of sediment is 0.85 mm. The specific gravity of the sediment is 2.65. The thickness of active layer is set to 0.01 m. The sediment transport formulas used in the simulations are Engelund-Hanson equation (EH), Meyer-Peter-Muller equation (MPM), WILCOCK equation, YANG73 equation, and YANG79 equation. The Manning's roughness coefficient is set to 0.035 in all the simulations.

1.2.2.4 Initial and Boundary Conditions

The simulation is a steady state solution, and the "AUTO" type initial condition is used in the simulation. The total discharge boundary condition, $Q = 0.035$ m^3/s, is set at the inlet boundary. And the outlet boundary is the constant water surface elevation (h = 0.2 m).

1.2.2.5 Simulated Results

The simulated results of bed bathymetry are shown in Fig.1.11. The simulated bed bathymetry using the revised model under-estimated the scour depths around the spur dikes (Fig.1.11b). However, the revised model predicted a deeper scour hole around the second dike, but a shallower scour hole around the first dike (Fig.1.11c). In general, the revised model under-predicted the scour depth around the first dike, but better predicted the scour depth around the second dike. Neither the previous nor the revised model's results closely matched the measurements.
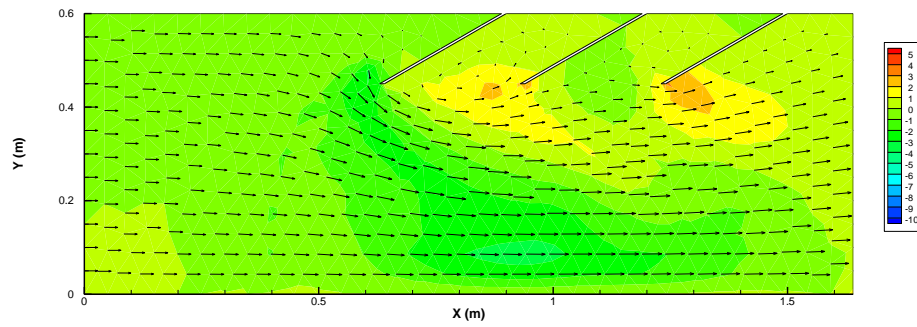
a. Simulated bed bathymetry (cm) using the revised model
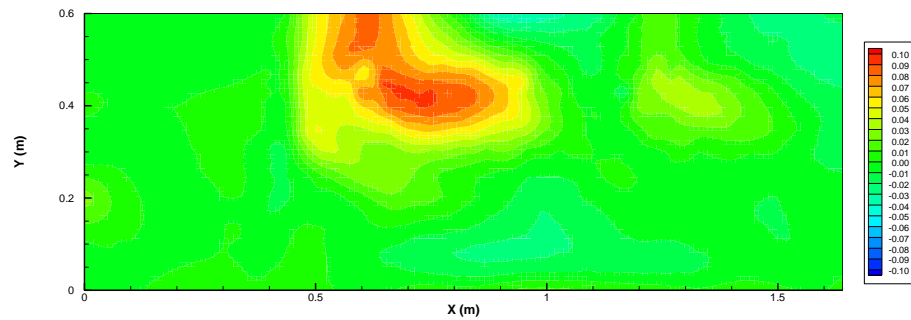
b. Difference (m) of simulated and measured bed elevations (simulated – measured)
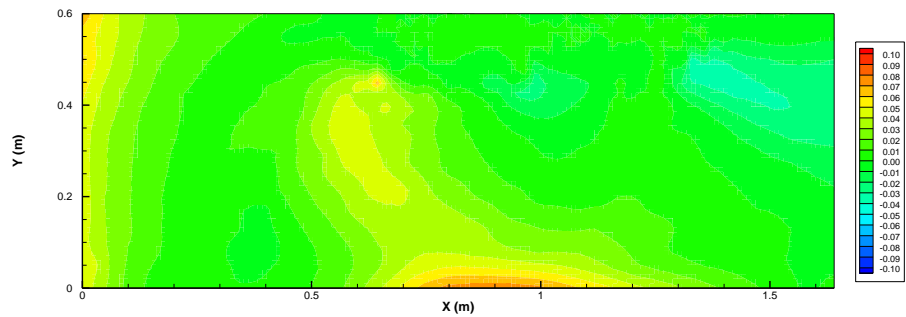
c. Difference (m) of simulated bed elevations compared with the results from the previous version (new - old results from SRH2D model).

Fig.1.11 Results of bed bathymetry using the revised SRH2D model

The revised SRH2D model predicted the maximum TKE occurred at the tip of the second dike, which is consistent with the experimental measurements (Fig.1.12a). The updated SRH2D model predicted larger TKE than the previous model (Fig.1.12b).
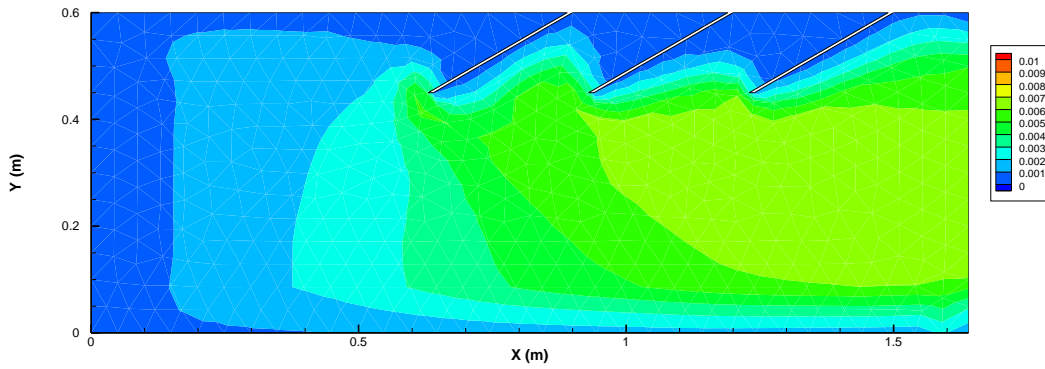
a. Simulated TKE distribution using the revised SRH2D model
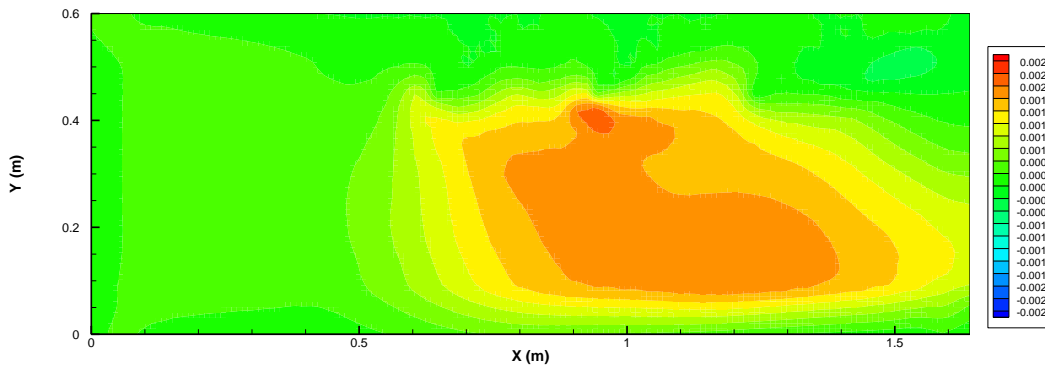
b. Differences between results of revised and previous SRH2D model (new-old)

Fig.1.12 Results of simulated TKE distributions

The comparison of the simulated TKE from the revised SRH2D model and FLOW3D are shown in Fig.1.13. The results from the revised SRH2D model are better than those from the previous model, but not as good as the results from FLOW3D model. This perhaps is the limitation of depth-averaged two dimensional model.
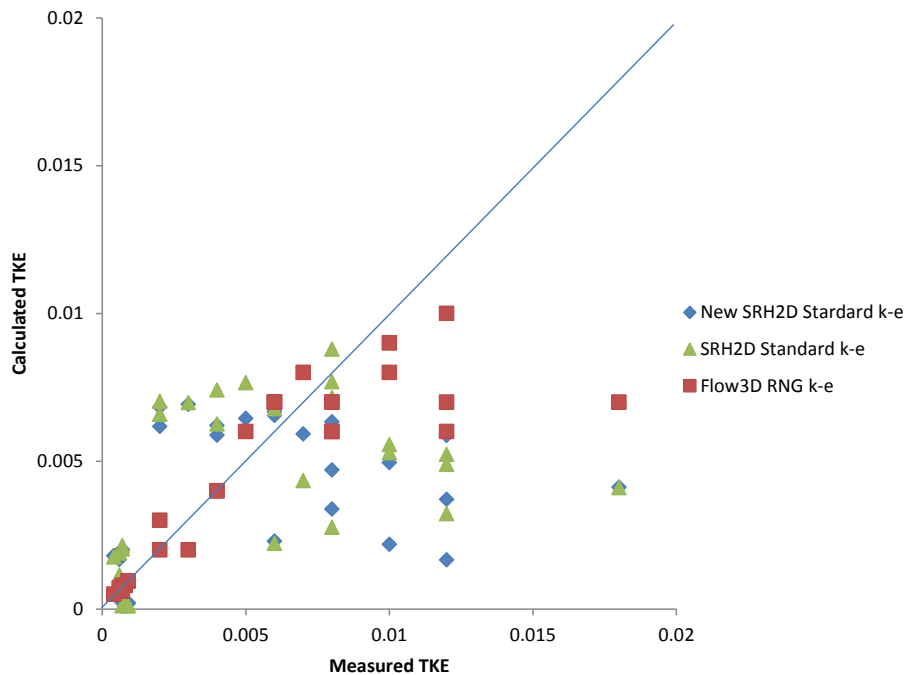
Fig.1.13 Comparisons of measured TKE with the simulated results from SRH2D k-e model and FLOW3D RNG k-e model.

1.2.2.6 Summary

The updated SRH2D model has improved the prediction of TKEs and better predicted the maximum scour depth near the second dike, but still cannot match the measurements and FLOW3D predicted TKEs.

1.3 Sediment Model Verification: Dam Break Flow over Mobile Bed

This test case is a benchmark experiment (NSF-PIRE project "Modelling of Flood Hazards and Geomorphic Impacts of Levee Breach and Dam Failure") carried out at UCL-Belgium to investigate the 2D morphological evolution of a mobile bed under dam-break flow [*Soares-Frazao et al.*, 2012]. The objective is to provide a test case to validate numerical models for the simulation of dam-break flow over a mobile bed.

The plan view of the flume is shown in Fig.1.14. The flume is 3.6 m wide and about 36 m long. The partial dam-break is represented by rapidly lifting the 1 m wide gate between two impervious blocks. The experiment lasted 20 s. Then, the gate was closed and the flow was

stopped. There are 8 gauges in the flume. Their exact positions are stated in [*Soares-Frazao et al.*, 2012].
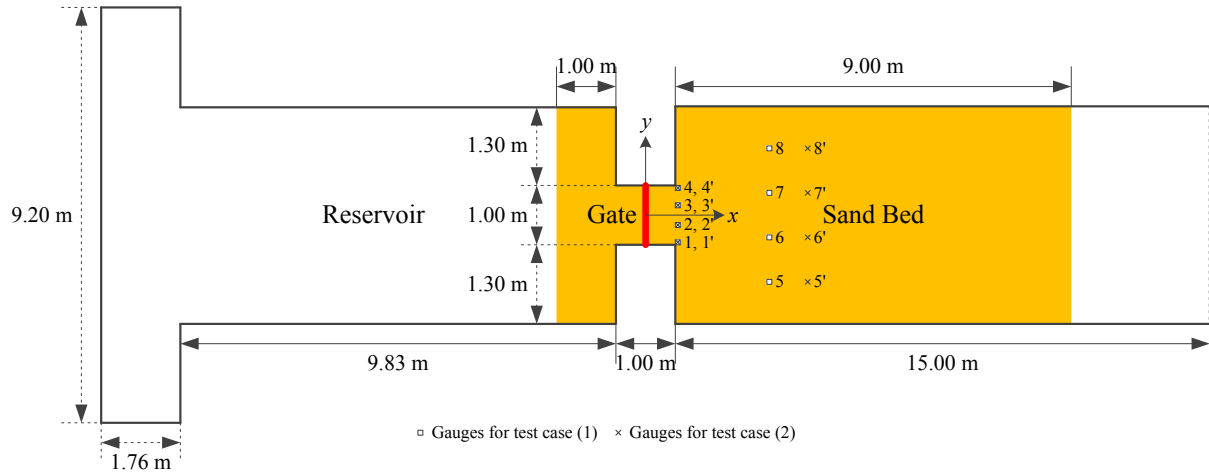
Fig.1.14 Experimental Setting

1.3.1 Model Set-up

The initial conditions are $h = 0.51m$ in the upstream reservoir and $h = 0.15m$ in the downstream channel. The boundary conditions are exit for the outlet and wall boundaries for all other boundaries. The following parameters are used in the simulation: sediment particle density $\rho_s = 2630kg/m^3$; median size $d_{50} = 1.61mm$; bed porosity $\phi = 0.4$; Manning coefficient $n = 0.0165$. Flow initial velocity is zero. Sediment size is 0.5 mm uniform sediment. Turbulence model is parabolic turbulence model. Sediment transport simulation is equilibrium transport model. The Yang73 total load transport formula is used. The time step is 0.01 sec, and the grid is triangular with an approximate size of 10 cm. It takes about 5 mins for each run.

1.3.2 Results

Flow field shown in Fig.1.15, the velocity field nearly matched the experimental observations.
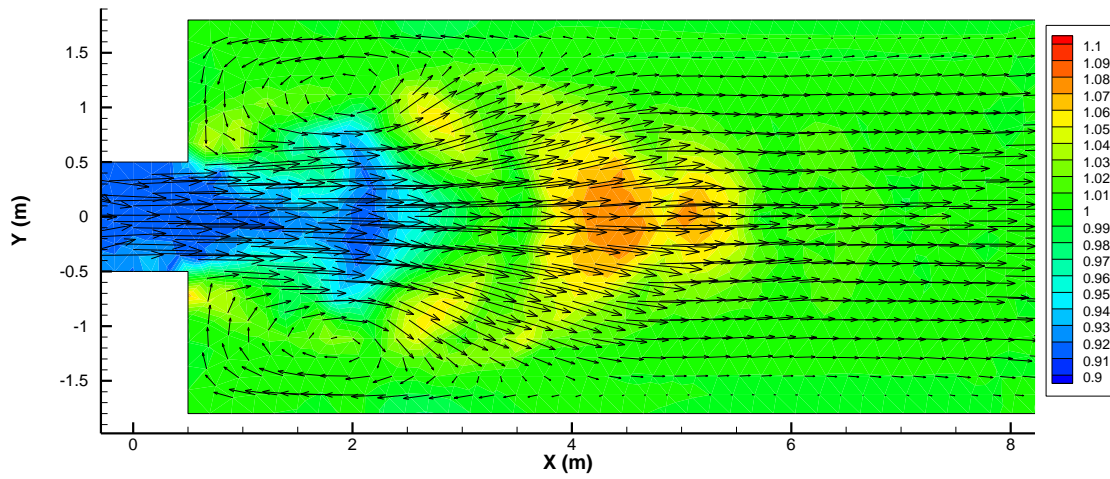
Fig 1.15 Bed elevation (m) with velocity vector field.
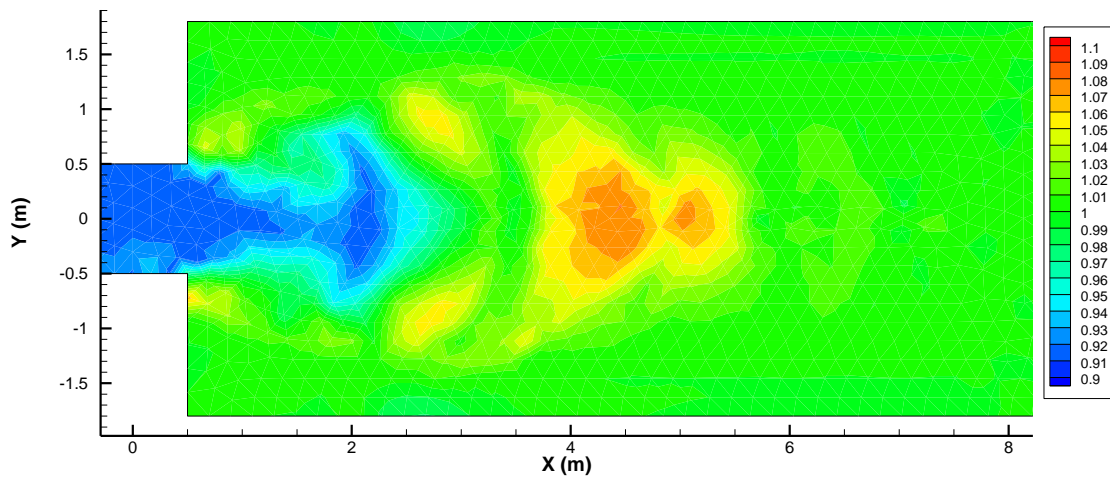
Fig.1.16 Bed elevation without velocity vector

Bed elevation shown in Fig.1.16, is promising showing deposition and erosion patterns around the gate.   The results of water surface elevation and bed elevations are compared with the measurements in Fig.1.17 and Fig.1.18. For water surface elevation, the RSME error at Gauge 3 is 0.0219 m, at Gauge #4 is 0.0259 m, Gauge #7 is 0.0298 m, Gauge #8 is 0.0356 m. For bed elevation, the RSME at y= 0.2m, 0.7m, and 1.45m are 0.0324 m, 0.0204 m, and 0.0152 m.
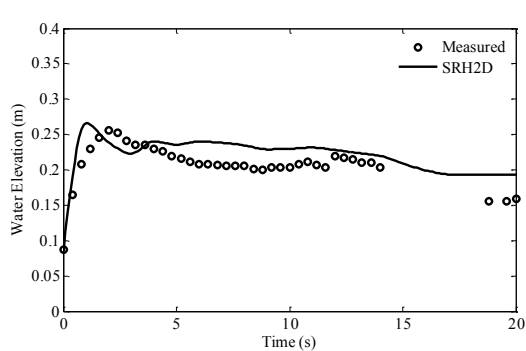
Gauge #3 (RMSE=0.0219m)
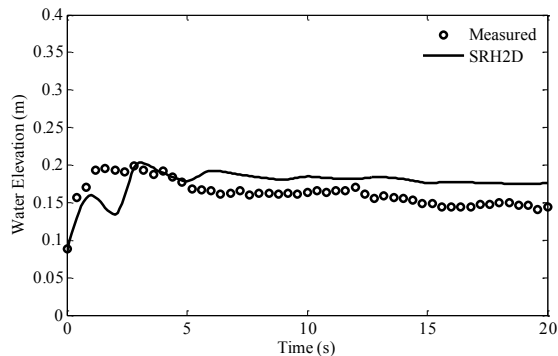
Gauge #4 (RMSE = 0.0259 m)
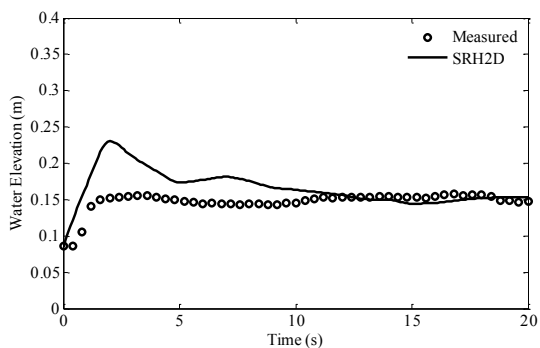
Gauge #7 (RMSE = 0.0298 m)
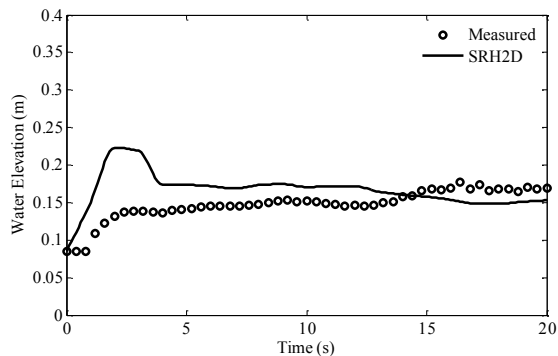
Gauge #8 (RMSE = 0.0356 m)

Fig.1.17 Comparison of simulated and measured water surface elevations
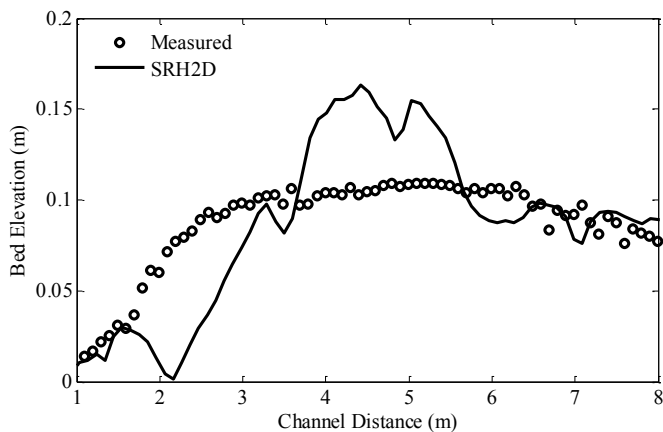
y = 0.2 *m*, RMSE = 0.0324 *m*
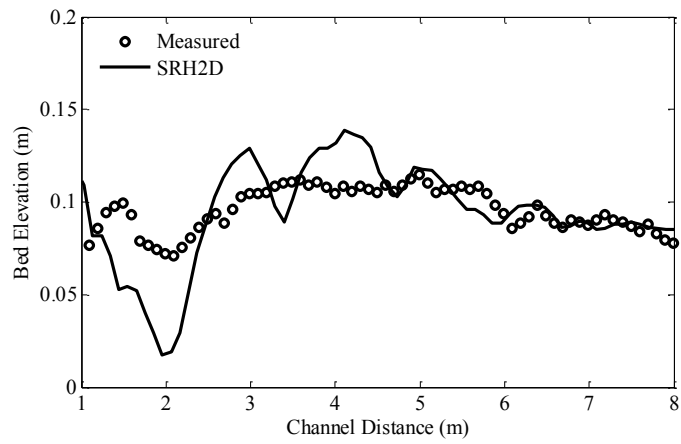
y = 0.7 *m*, RMSE = 0.0204 *m*
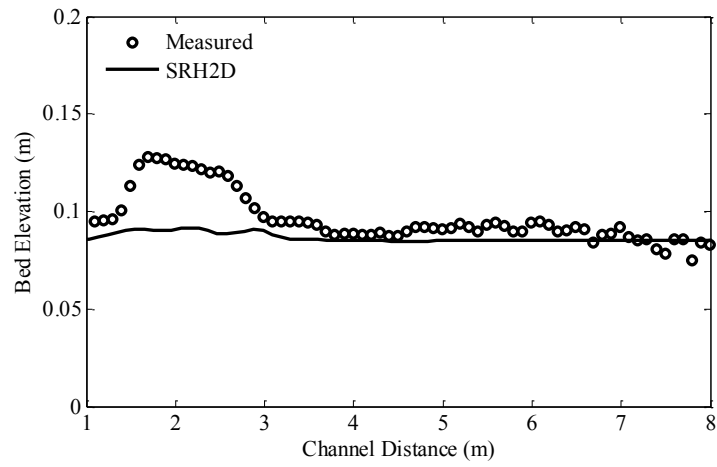
y = 1.45 *m*, RMSE = 0.0152 *m*

Fig.1.18 Comparison of simulated and measured bed elevations

Part 2: Simulation of Lake Mills Drawdown Experiment Using SRH2D Model

2.1 Introduction

The objective of this study is to simulate fluvial processes during the 1994 Lake Mills drawdown experiment in the Elwha River, Washington. The experiment drawdown was performed in April 1994 by gradually lowering the Lake level by 18 feet over one week period. Flow discharge, cross sectional data, and sediment size distribution were collected at the reservoir reach during the drawdown experiment. This study simulated the experimental drawdown using SRH2D model and compared the simulated results of cross sectional changes with measurements. We conducted two series of simulations: one is to use the measured data to extract cross sections, and then test the sensitivities of modeling results to meshes, roughness coefficient, various sediment transport formulas, and different methods of adaptive lengths; the other is to use a refined mesh with many breaklines to pre-define the channel flow. Those two series of simulations are summarized in Section 2.2 and 2.3, respectively.

2.2 Model Initial Run and Sensitivity Test

2.2.1 Computational Grid

The simulation domain is the Lake Mills reservoir reach covering the reservoir delta from Section 3 to Section 17 as shown in Fig.2.1 and 2.2. The simulation boundary including the left and right banks is obtained from the boundaries of measured cross sections. The bathymetry in the simulated reach is interpolated using the surveyed bed elevation at each cross sections in 1994.
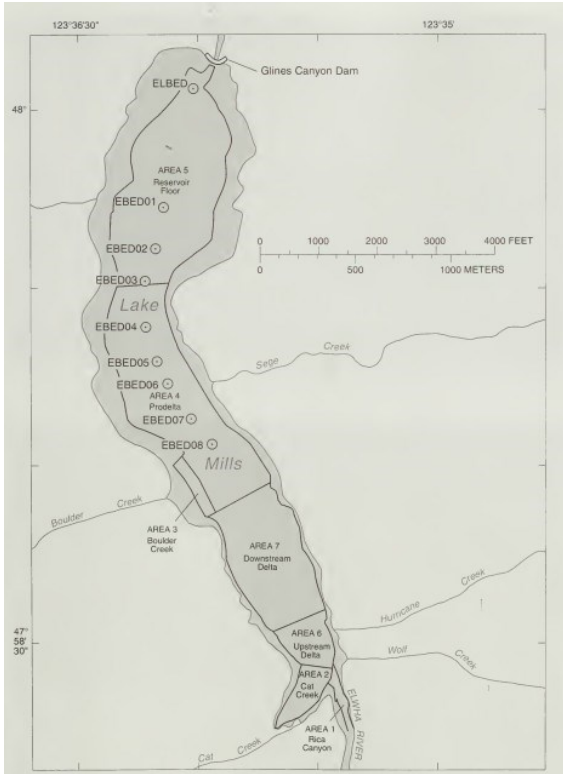
Fig.2.1 Location of the simulation reach.　　**Fig.2.2** Location of surveyed cross sections
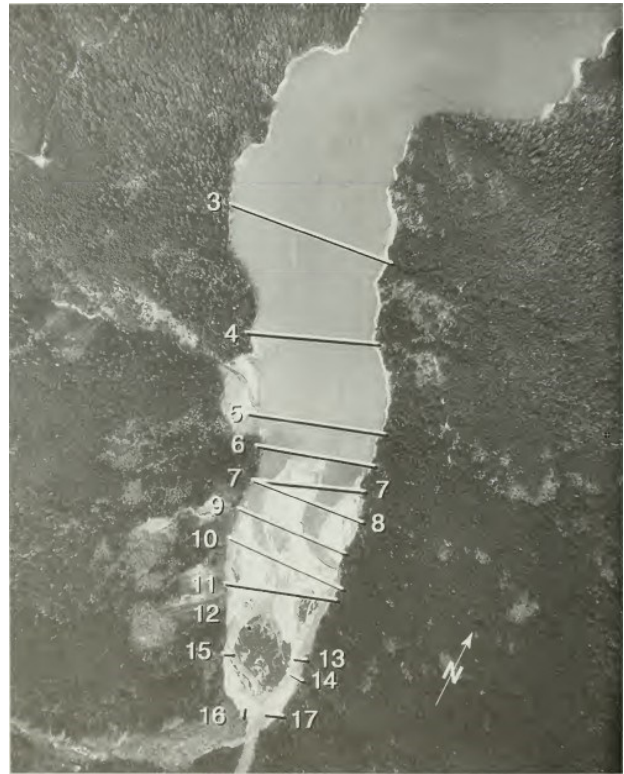
This study used three computational meshes with a spacing of 30, 15, and 10 m shown in Fig.2.3, respectively.
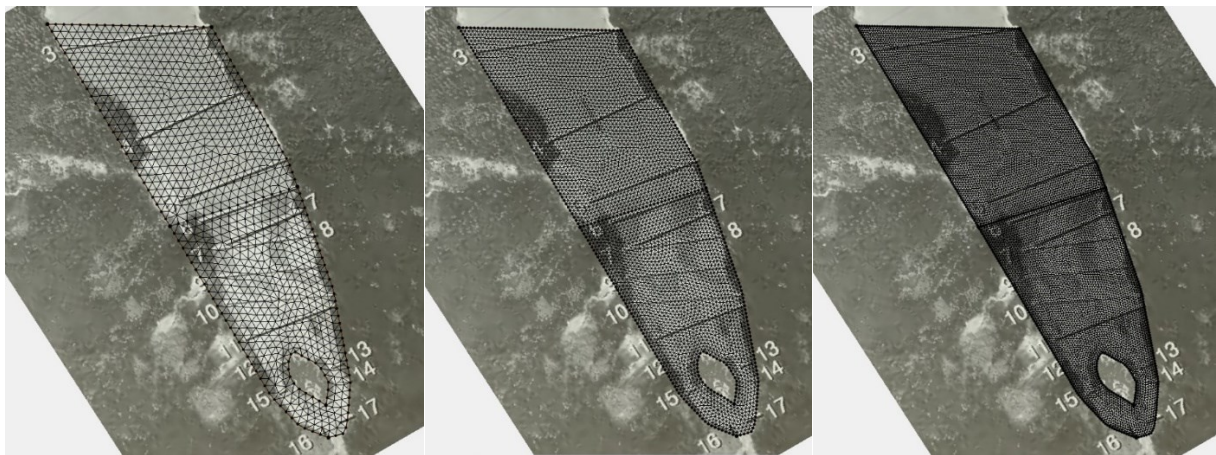
Fig.2.3 Computational grid with 30m, 15m, and 10m spacing

2.2.2 Simulation Data

Stream flow data were collected at five sites. Daily flows at ELWW, a gaging station that was established just a few weeks prior to the beginning of the drawdown experiment. The

ELWW gage site was established to provide stream flow discharge and total sediment discharge upstream from the Lake Mills Delta. A staff gage and temporary recording gage with submersible pressure sensor were installed at this site. The stream flow discharge (Fig.2.4) and sediment discharge (Fig.2.5) measured at ELWW gage were used.
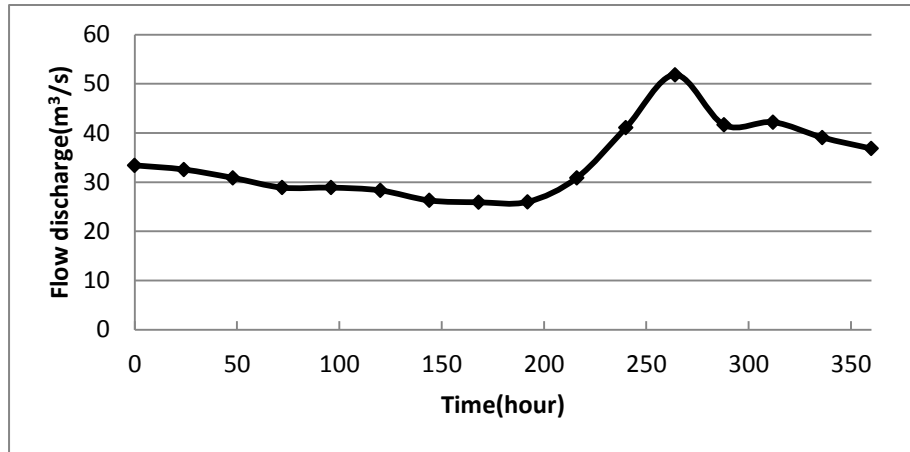
Fig.2.4 Stream flow discharge
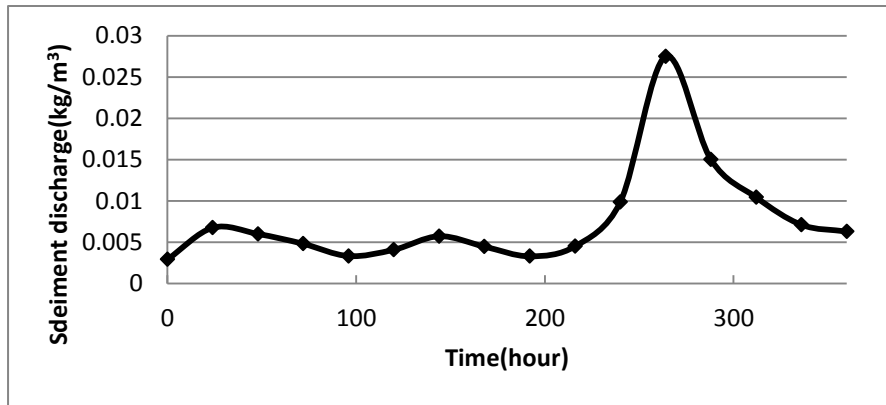
Fig.2.5 Sediment discharge

The lake drawdown began with a full lake at 8:00 am on April 9, 1994. During the experiment, the lake's water level was lowered 18 feet over a 1-week period from April 9 to 16. Drawdown rates were about 3 feet per day for the first 5 days, for a total of 15 feet. The lake was drawn down 2 feet between April 14 and 15 and 1 foot between April 15 and 16. A drawn down of 18 feet was reached 8:00 am on April 16, and then held at constant elevation for a week. The

changes of lake level are shown in Fig.2.6, and were used as the downstream boundary condition. The particle-size distribution collected at ELD1 station was used. The distribution curve is shown in Fig.2.7.
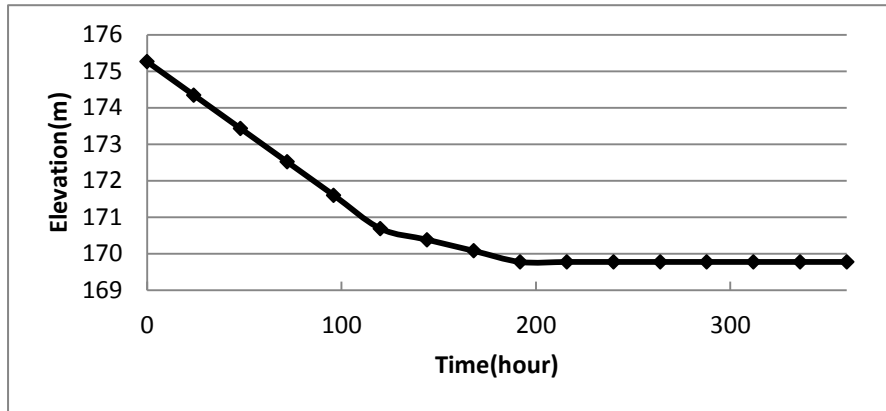
Fig.2.6 Downstream boundary conditions
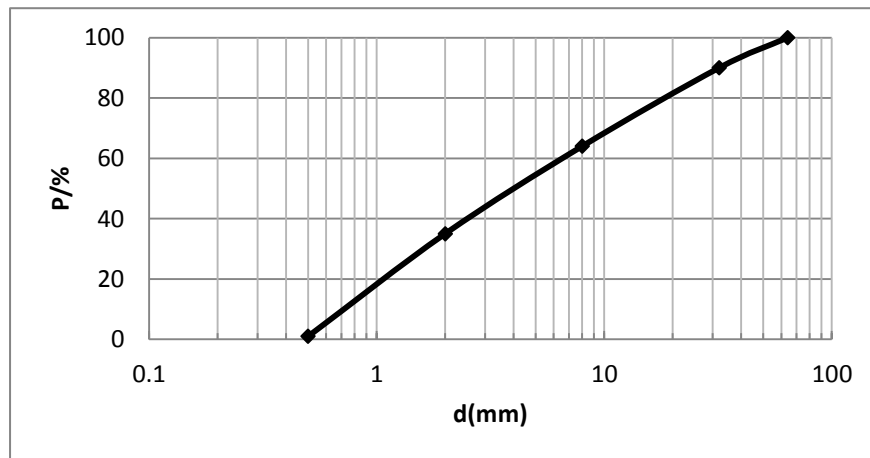
Fig.2.7 Particle-size distribution

The time step used for the three computational meshes is 5.0 s. The total simulation time is 360 hours. When the mesh size is decreased to 8 m, the SRH2D doesn't converge even reducing the time step to 0.01 s.

2.2.3 Simulated Results

The simulated bed elevations using three different meshes were compared with the measurements on April 16th and April 23th, and shown in Fig.2.8 and 2.9, respectively. On April 16, the model over-estimated erosion at Section 6, while unable to capture the two channels

formed on the delta from Section 7 to 11. From Section 12 to 17, simulated results are closer to the measurements except at Section 15 and 17.

2.8a. Cross-section 6(April 16th).
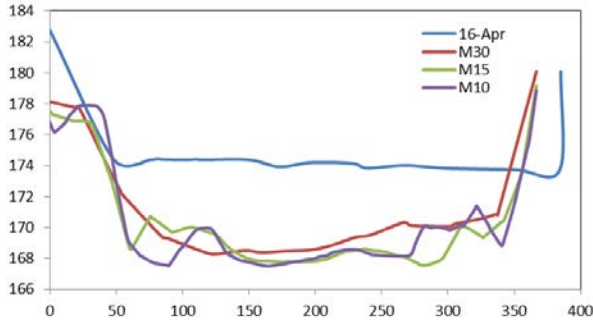
2.8b. Cross-section 7(April 16th)
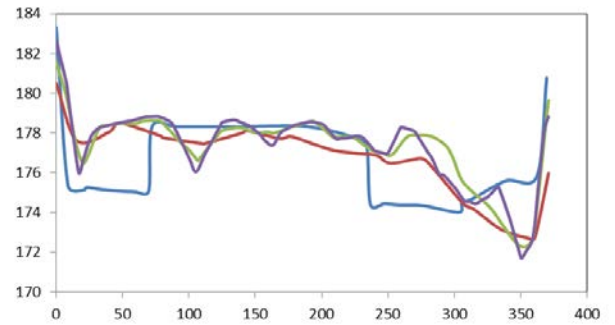
2.8c. Cross-section 8(April 16th).
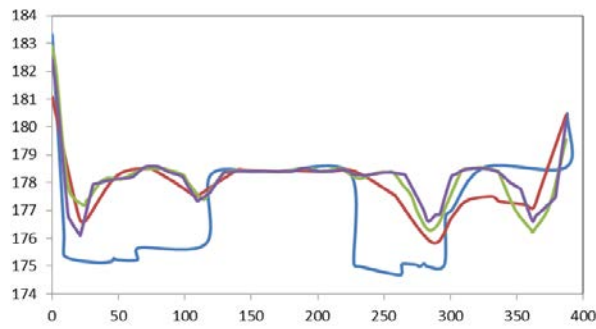
2.8d. Cross-section 9(April 16th).
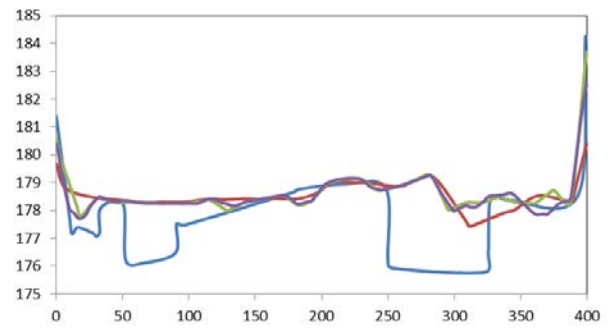
2.8e. Cross-section 10(April 16th).
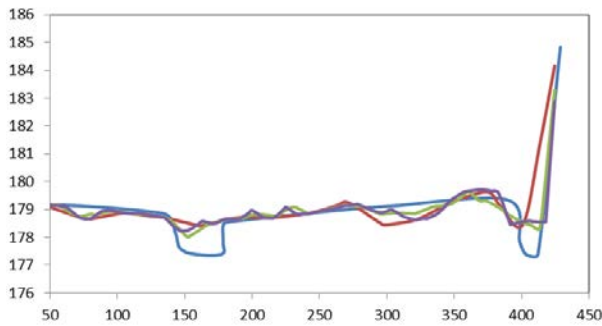
2.8f. Cross-section 11(April 16th).
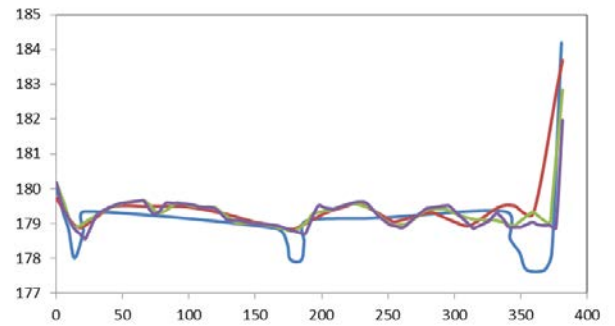
2.8g. Cross-section 12(April 16th).　　　**2.8h.** Cross-section 13(April 16th).
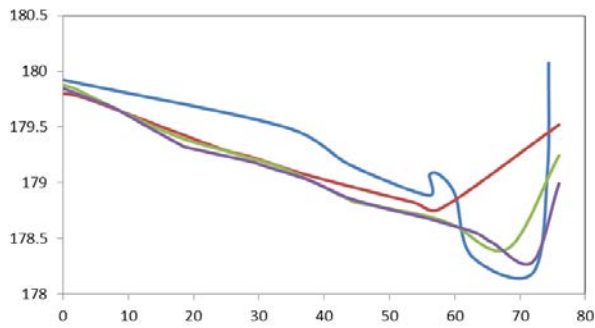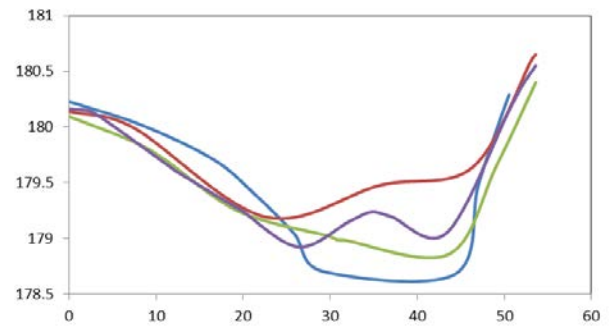
2.8i. Cross-section 14(April 16th).　　　**2.8j.** Cross-section 15(April 16th).
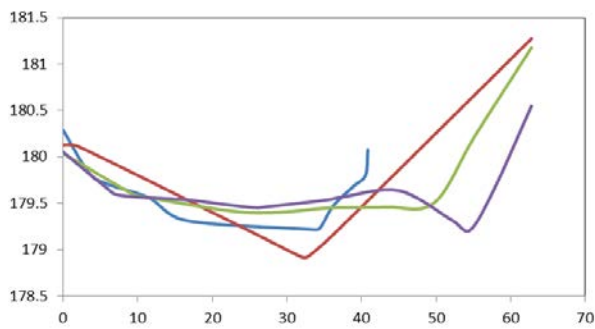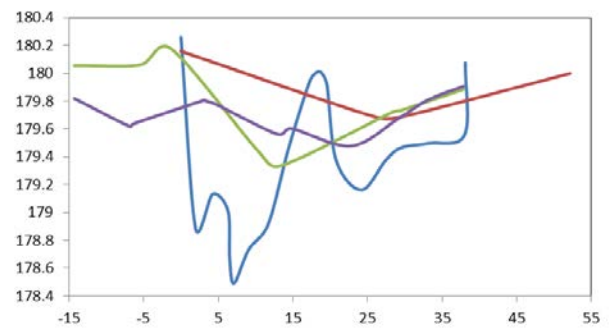
2.8k. Cross-section 16(April 16th).　　　**2.8l.** Cross-section 17(April 16th).
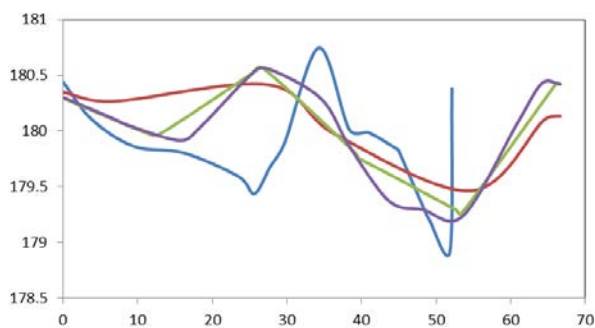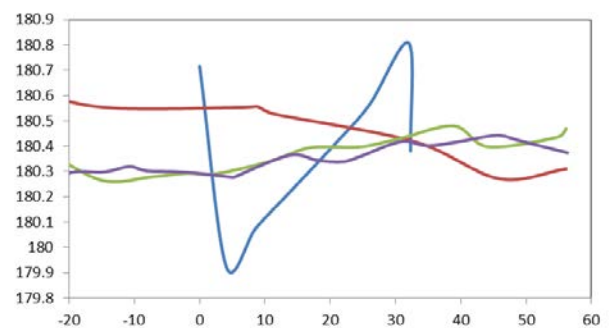
Figure 2.8 Simulation results of cross-sections on April 16th

2.9a. Cross-section 3(April 23th).
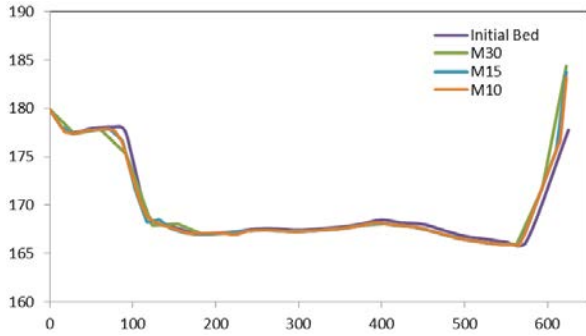
2.9b. Cross-section 4(April 23th).
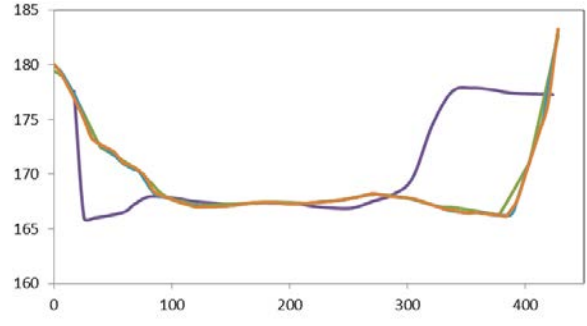
2.9c. Cross-section 5(April 23th).
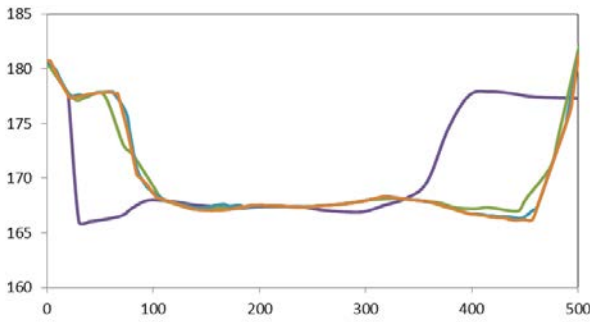
2.9d. Cross-section 6(April 23th).
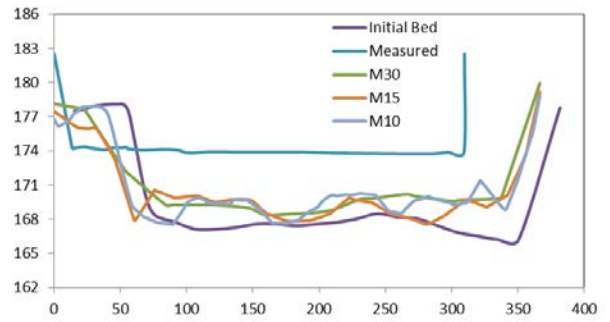
2.9e. Cross-section 7(April 23th).
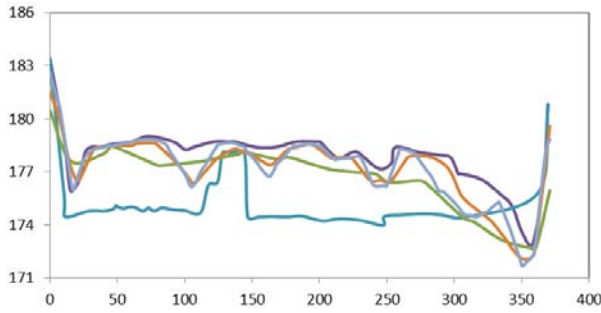
2.9f. Cross-section 8(April 23th).
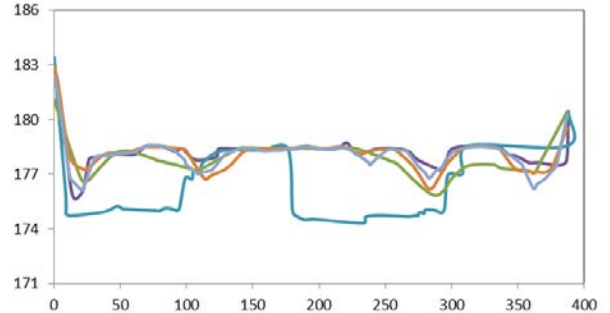
2.9g. Cross-section 9(April 23th).
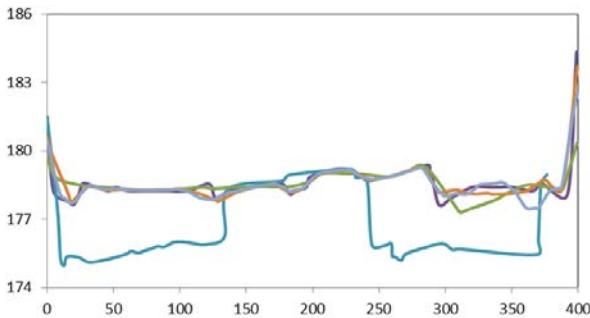
2.9h. Cross-section 10(April 23th).

2.9i. Cross-section 10 (April 23th).
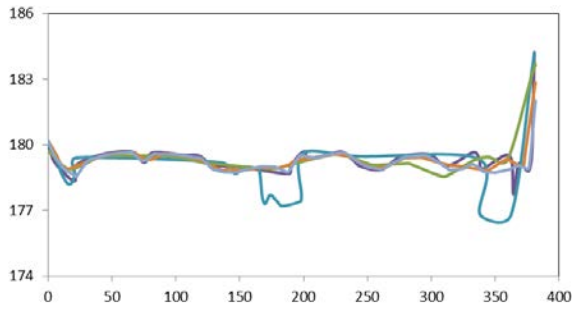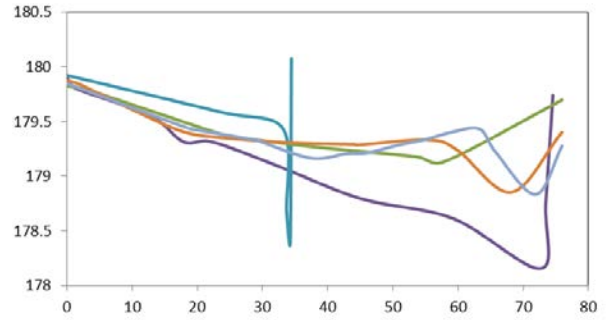
2.9k. Cross-section 13 (April 23th).
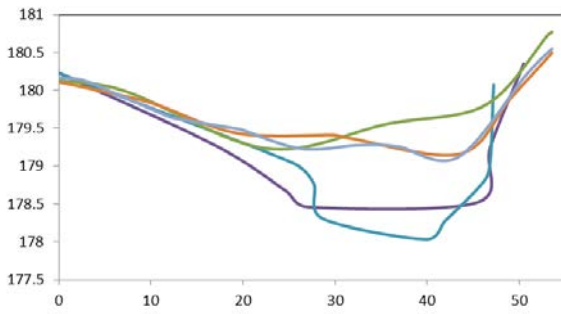
2.9l. Cross-section 14 (April 23th).
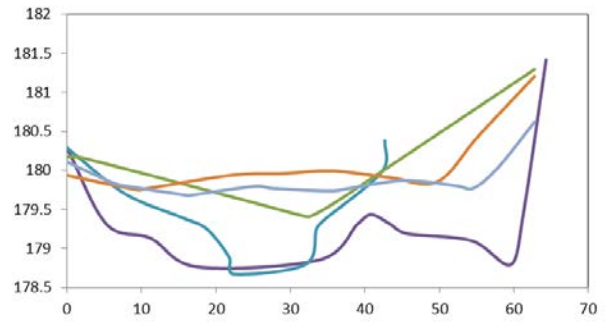
2.9m. Cross-section 15 (April 23th).
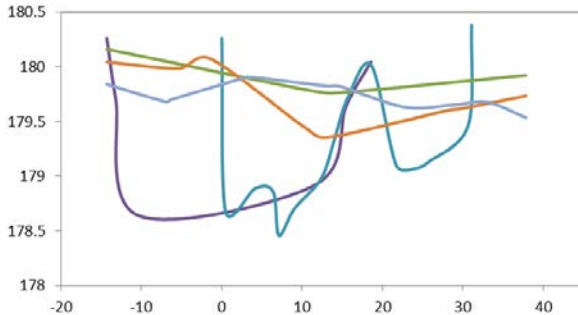
2.9n. Cross-section 16 (April 23th).
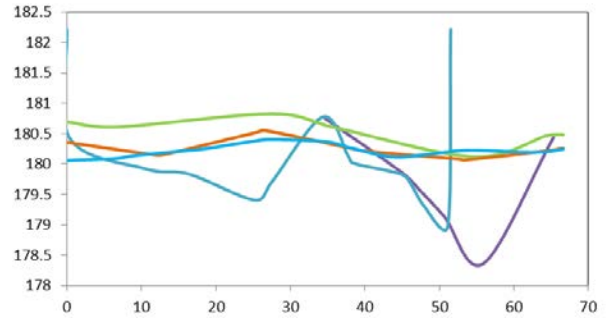
2.9o. Cross-section 17(April 23th).
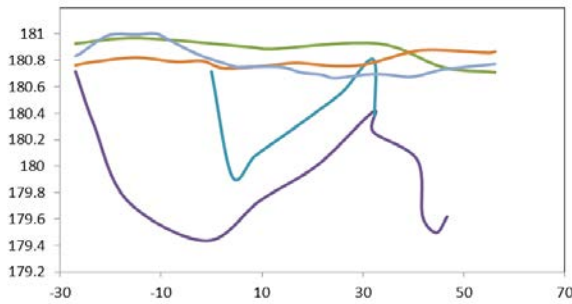
Figure 2.9a-o. Comparisons of different cross sections bed elevation at the end of the experiment (April 23th).

The final results at Section 3, 4, and 5 are the same regardless of mesh sizes, while no erosion occurred in those sections. At Section 6, the simulated results underestimate the deposition occurred. From Section 7 to 11, two large channels are formed at both sides of the delta, while the simulated results have several channels formed on the delta, but cannot match the observed channels. From Section 12 to 17, the simulated results considerably over-estimated the deposition comparing to observed bed elevation.

The errors of simulated bed elevation changes may due to 1) inaccurate bathymetry data; 2) bank erosion induced channel changes have not been simulated; 3) avulsion or bifurcation processes may also need to be considered.

Additionally, the simulated flow discharge at ELD1 and ELD2 are compared with the gage records. The locations of ELD1 and ELD2 are also estimated based on the map. Since there is no discharge output directly from SRH2D model, we used discharges at Section 8 and 10 to approximate discharges at ELD2 and ELD1, respectively. The discharges at Section 8 and 10 were calculated by integrating the product of flow area and depth-averaged velocity. The simulated discharges are compared with gage measurements in Fig.2.10, which showed significant overestimate of discharge. This perhaps attributes to the fact that the gage installed at the right side of the delta only record the flow at the right side channel. However, the calculated discharge from simulated results accounted flows in both branches.

(a) ELD1   (b) ELD2
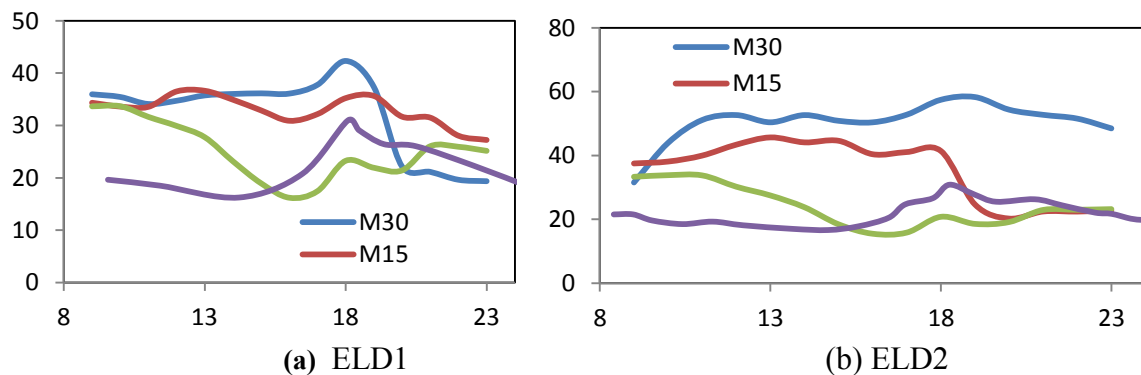
Figure 2.10 (a-b). Comparisons of stream flow discharge in ELD1 and ELD2.

2.2.4 Sensitivity of Modeling Results

SRH2D model allows for both triangular and quadrilateral grid, and has six sediment transport equations available. The modeling results can be sensitive to the selection of mesh, sediment transport equation, Manning's coefficient, and adaptation length for bed load transport. The following sections summarized the results of sensitivity analysis.

2.2.4.1 Sediment Transport Formula

Figure 2.11 is the results of bed elevation changes at surveyed cross sections using six different sediment transport formulas. Results from all the formulas are similar except for Yang (1973)'s relation. Using Yang (1973) relation, erosion is over-estimated at sections upstream of the delta, especially at Section 16 and 17.

2.11a. Cross-section 6.　　　　　　　　　**2.11b.** Cross-section 7
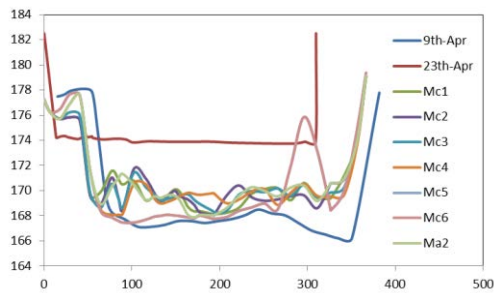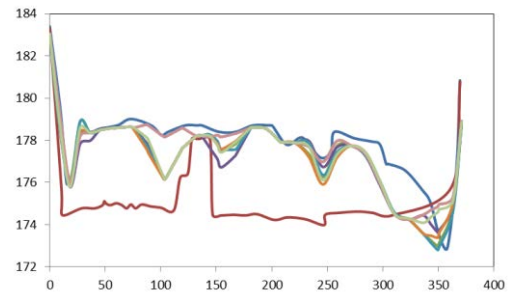
2.11c. Cross-section 8.　　　　　　　　　**2.11d.** Cross-section 9.
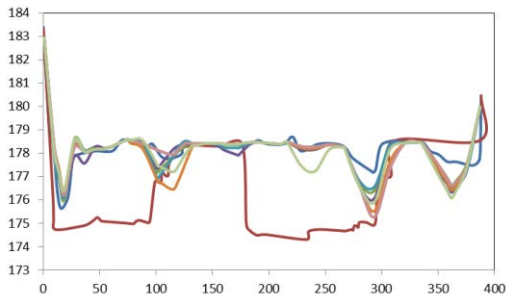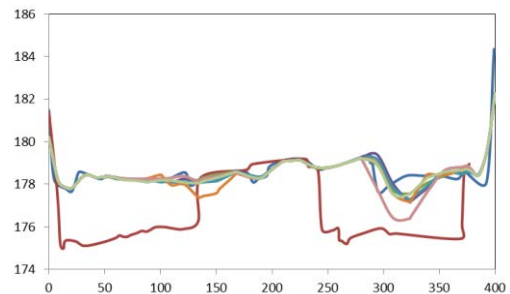
2.11e. Cross-section 10.　　　　　　　　　**2.11f.** Cross-section 11.
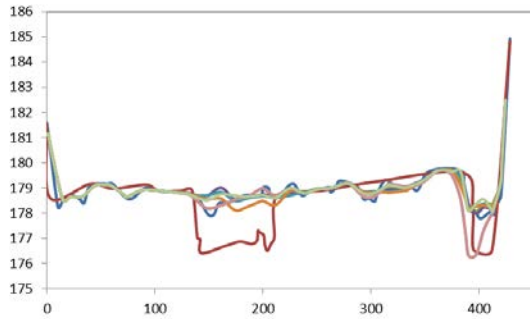
2.11g. Cross-section 12.
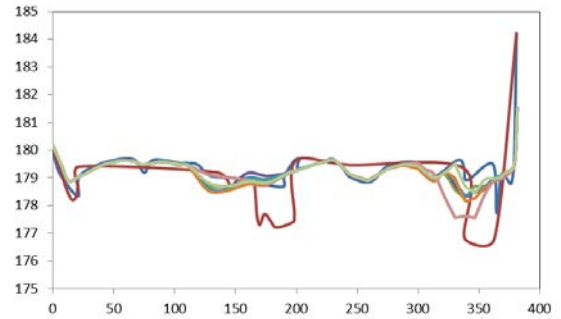
2.11h. Cross-section 13.
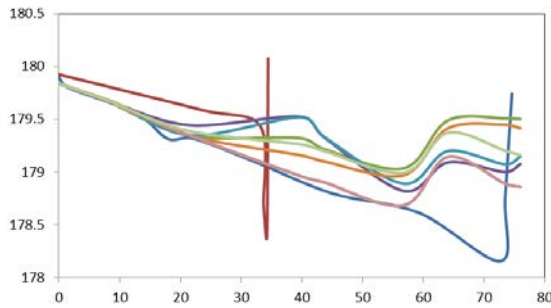
2.11i. Cross-section 14.
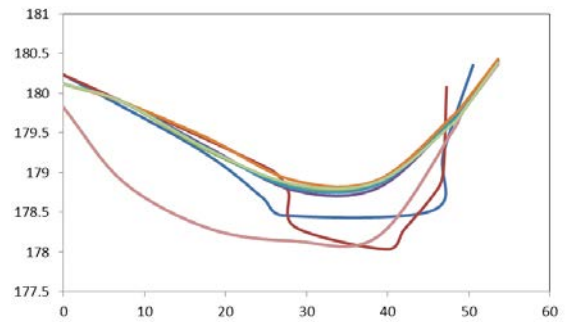
2.11j. Cross-section 15.
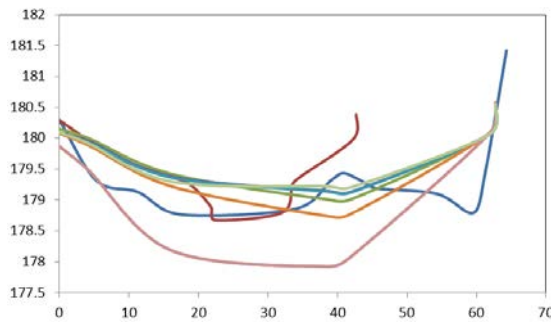
2.11k. Cross-section 16.
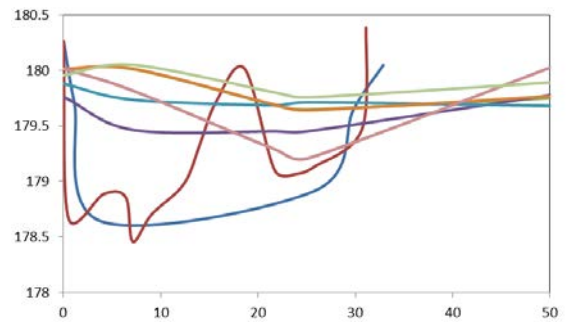
2.11l. Cross-section 17.
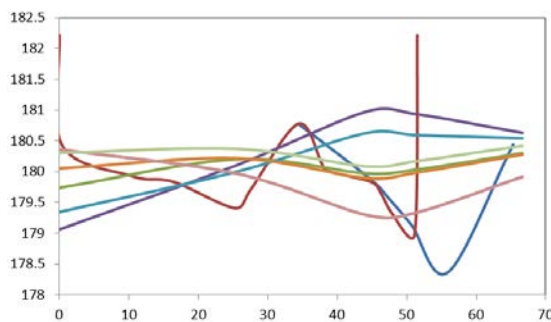
Fig.2.11 (a-l). Comparisons of different cross sections bed elevation using different sediment equations. Mc1: Engelund-Hansen (1972); Mc2:Parker (1990); Mc3: Wilcock-Crowe (2003) ; Mc4:Wu et al. (2000); Mc5:Yang (1973); Mc6:Yang(1979); Ma2: Meyer-Peter and Muller (1948).

2.2.4.2 Adaptation Length

Fig.2.12 shows the results of different adaptation lengths: 1m, 3m, and 5m. There is no difference of simulated bed elevations using three different adaptation lengths. All the lines collapsed in a single line in Fig.2.12.

2.12a. Cross-section 6.
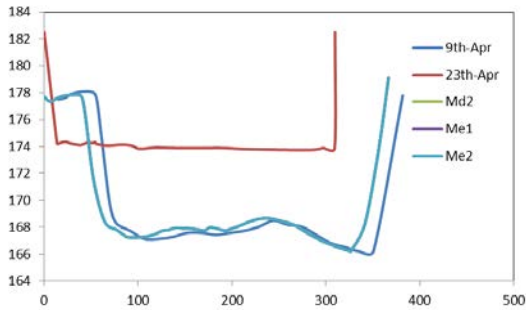
2.12b. Cross-section 7
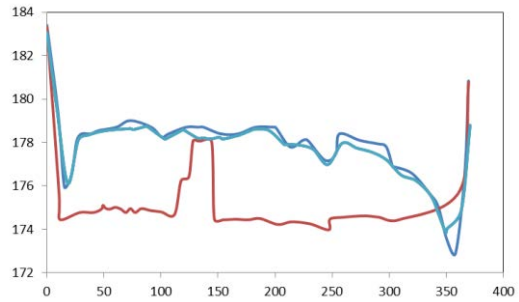
2.12c. Cross-section 8.
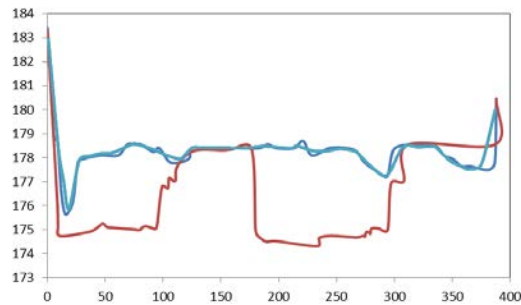
2.12d. Cross-section 9.
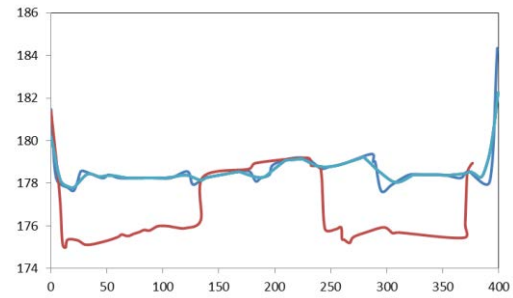
2.12e. Cross-section 10.
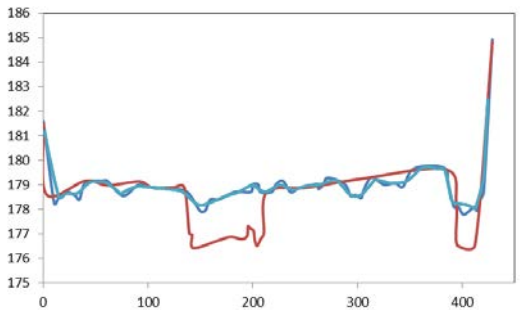
2.12f. Cross-section 11.
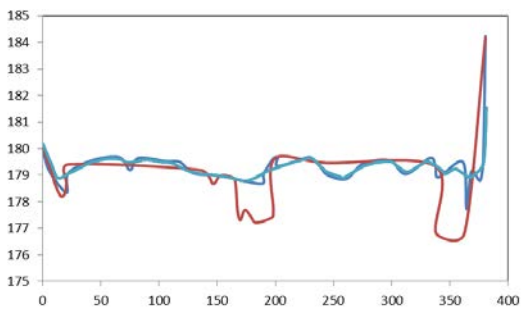
2.12g. Cross-section 12.

2.12h. Cross-section 13.
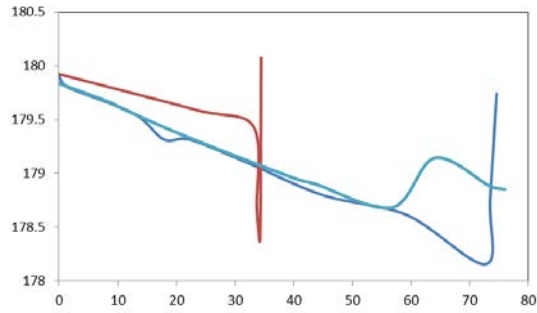
2.12i. Cross-section 14.
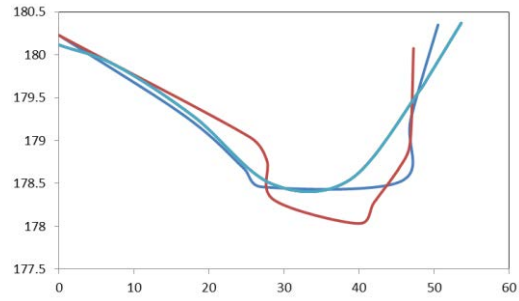
2.12j. Cross-section 15.
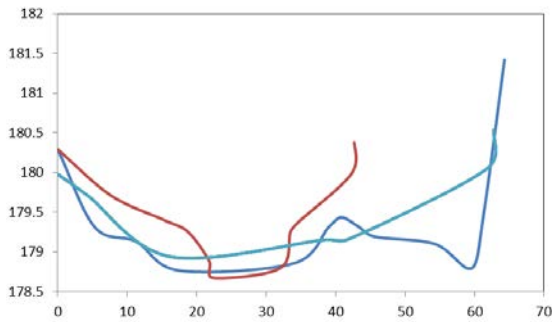
2.12k. Cross-section 16.
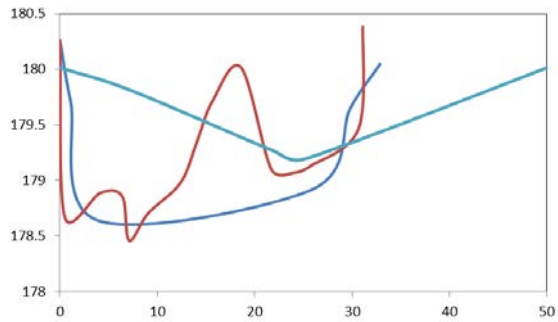
2.12l. Cross-section 17.
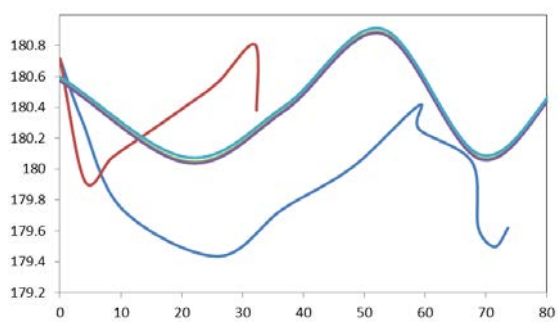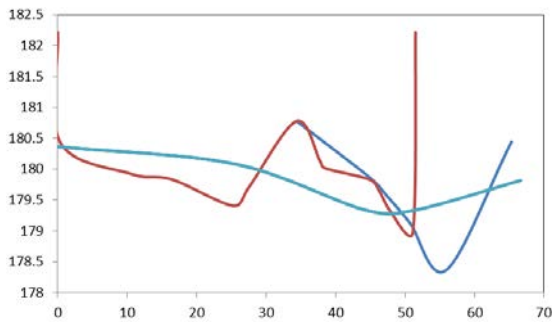
Fig.2.12 (a-l). Comparisons of different cross sections bed elevation using different adaptation length. Md2: Adaptation length is 3m; Me1: Adaptation length is 1m; Me2: Adaptation length is 5m.

2.2.4.3 Manning's Coefficient

The simulation zone is separated into four zones as shown in Fig.2.13. Six groups of roughness coefficients were assigned to those zones, and those values are:

Ma2: zone1-0.0155, zone2-0.0160, zone3-0.0165, zone4-0.0160;

Ma3: zone1-0.0130, zone2-0.0150, zone3-0.0165, zone4-0.0150;

Ma4: zone1-0.0150, zone2-0.0200, zone3-0.0270, zone4-0.0170;

Md1: zone1-0.0200, zone2-0.0400, zone3-0.0600, zone4-0.0200;

Md2: zone1-0.0300, zone2-0.0500, zone3-0.0600, zone4-0.0200;

Ma3: zone1-0.0400, zone2-0.0600, zone3-0.0100, zone4-0.0300;
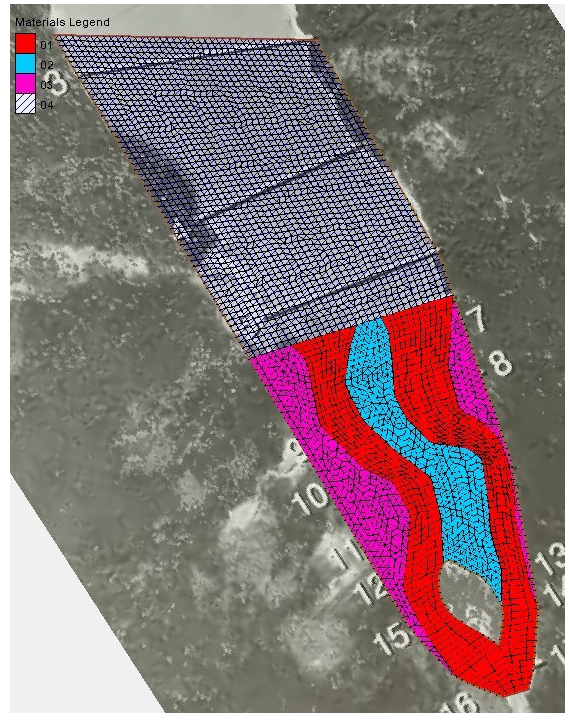
Fig.2.13 Four simulation zones of different roughnesses.
(zone 1 –red; zone 2 – blue; zone 3- pink; zone 4- black/white)

Simulated results of different roughness values are summarized in Fig.2.14. As roughness increases, more erosion is observed. The simulated results are sensitive to the selections of roughness coefficient.

2.14a. Cross-section 6.

2.14b. Cross-section 7
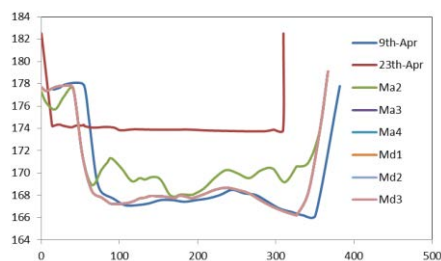
2.14c. Cross-section 8.
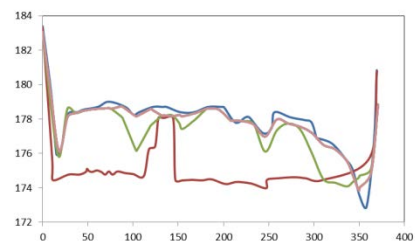
2.14d. Cross-section 9.
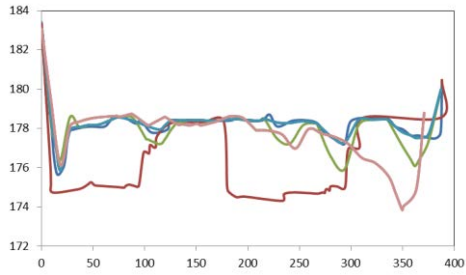
2.14e. Cross-section 10.
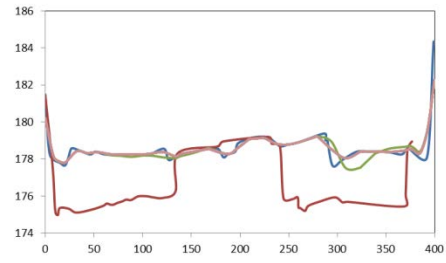
2.14f. Cross-section 11.
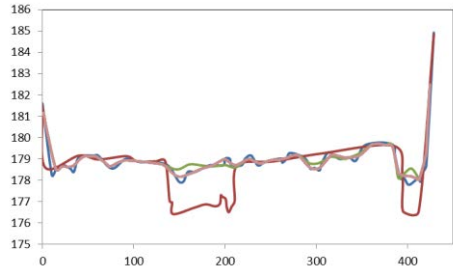
2.14g. Cross-section 12.
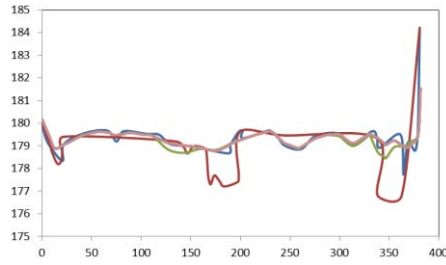
2.14h. Cross-section 13.
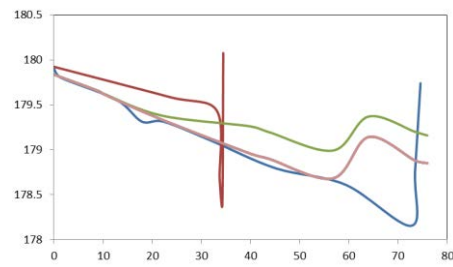
2.14i. Cross-section 14.
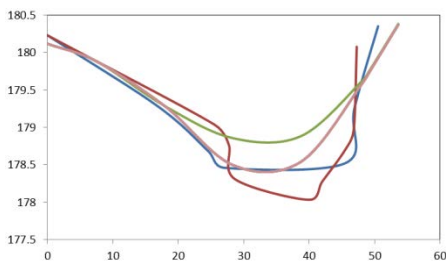
2.14j. Cross-section 15.
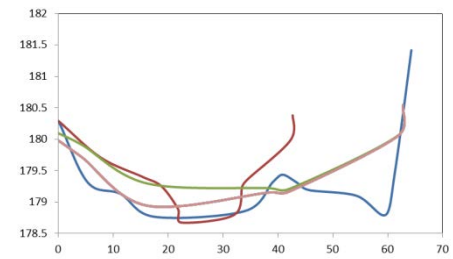
2.14k. Cross-section 16.
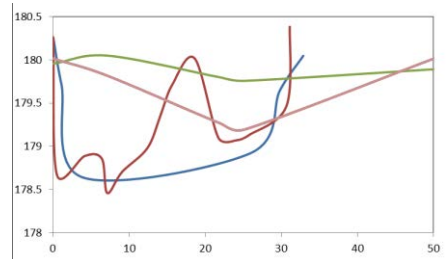
2.14l. Cross-section 17.
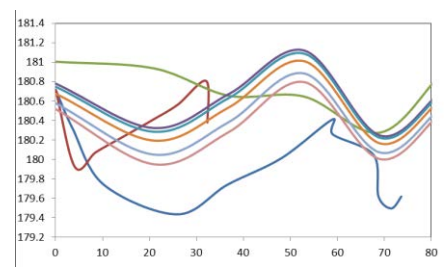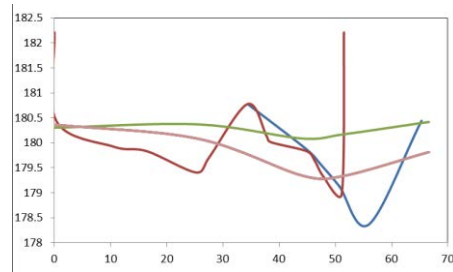
Figure 2.14 (a-l). Comparisons of different cross sections bed elevation using different Manning coefficient.

36

Ma2: zone1-0.0155, zone2-0.0160, zone3-0.0165, zone4-0.0160;

Ma3: zone1-0.0130, zone2-0.0150, zone3-0.0165, zone4-0.0150;

Ma4: zone1-0.0150, zone2-0.0200, zone3-0.0270, zone4-0.0170;

Md1: zone1-0.0200, zone2-0.0400, zone3-0.0600, zone4-0.0200;

Md2: zone1-0.0300, zone2-0.0500, zone3-0.0600, zone4-0.0200;

Ma3: zone1-0.0400, zone2-0.0600, zone3-0.0100, zone4-0.0300;

2.2.4.4 Mesh Type

The results of using two different meshes: one is pure quadrilateral, and the other is mixed triangular and quadrilateral (Fig.2.15), are shown in Fig.2.16. The results of using two different meshes are slightly different, but none of them tend to converge to the measurements. This indicates that the selection of mesh doesn't affect the results.
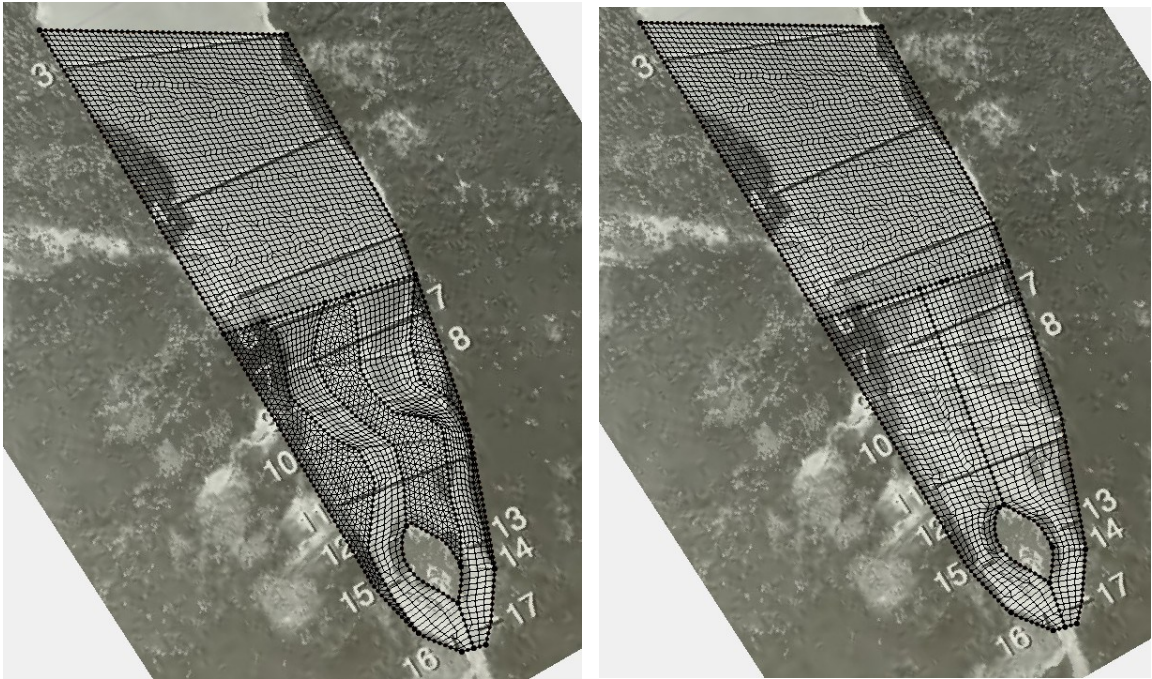
Fig.2.15. Two different meshes: (a) mixed mesh; (b) pure quadrilateral mesh

2.16a. Cross-section 6.
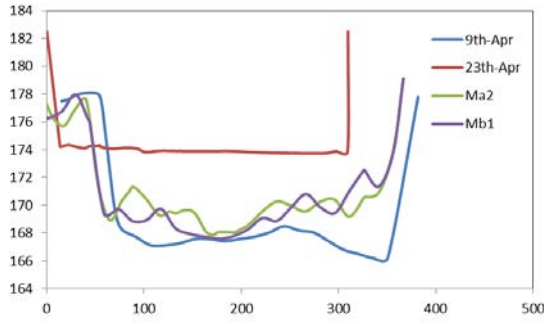
2.16b. Cross-section 7
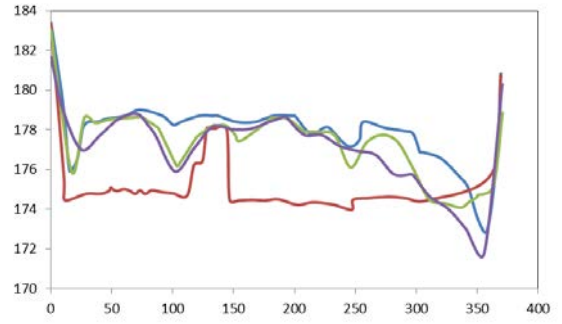
2.16c. Cross-section 8.
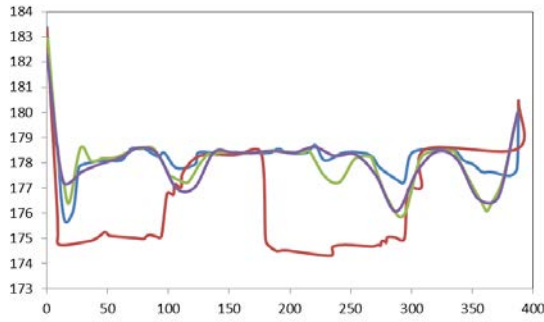
2.16d. Cross-section 9.
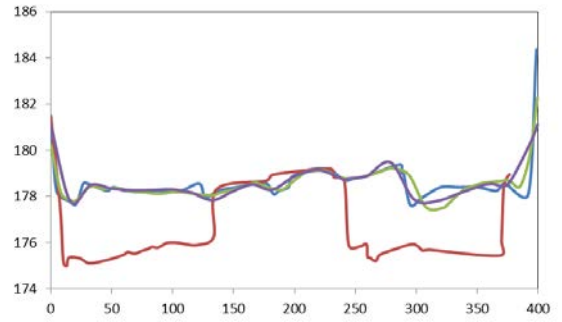
2.16e. Cross-section 10.
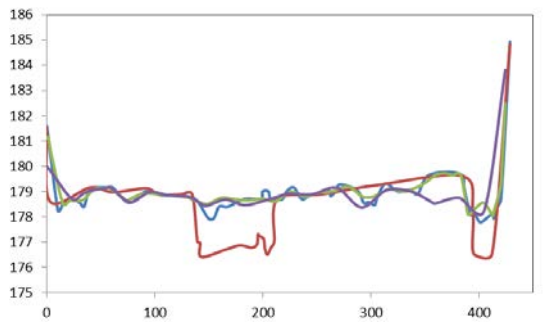
2.16f. Cross-section 11.
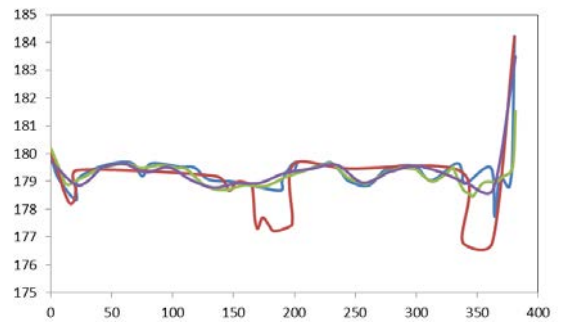
2.16g. Cross-section 12.

2.16h. Cross-section 13.

2.16i. Cross-section 14.　　　　　　　**2.16j.** Cross-section 15.

2.16k. Cross-section 16.　　　　　　**2.16l.** Cross-section 17.
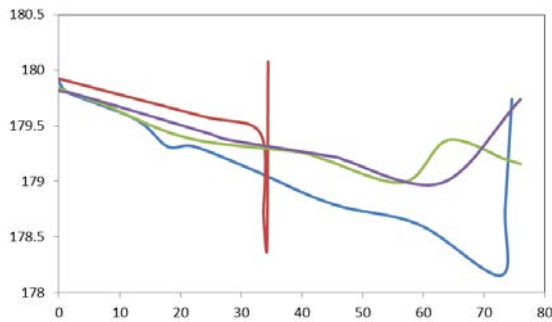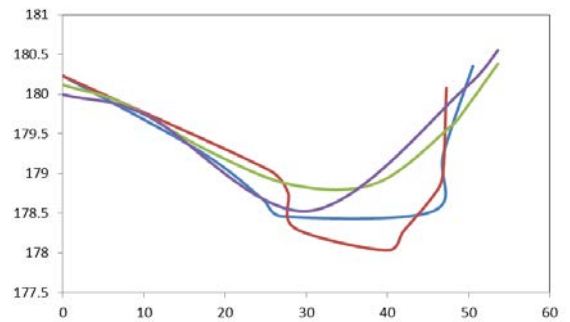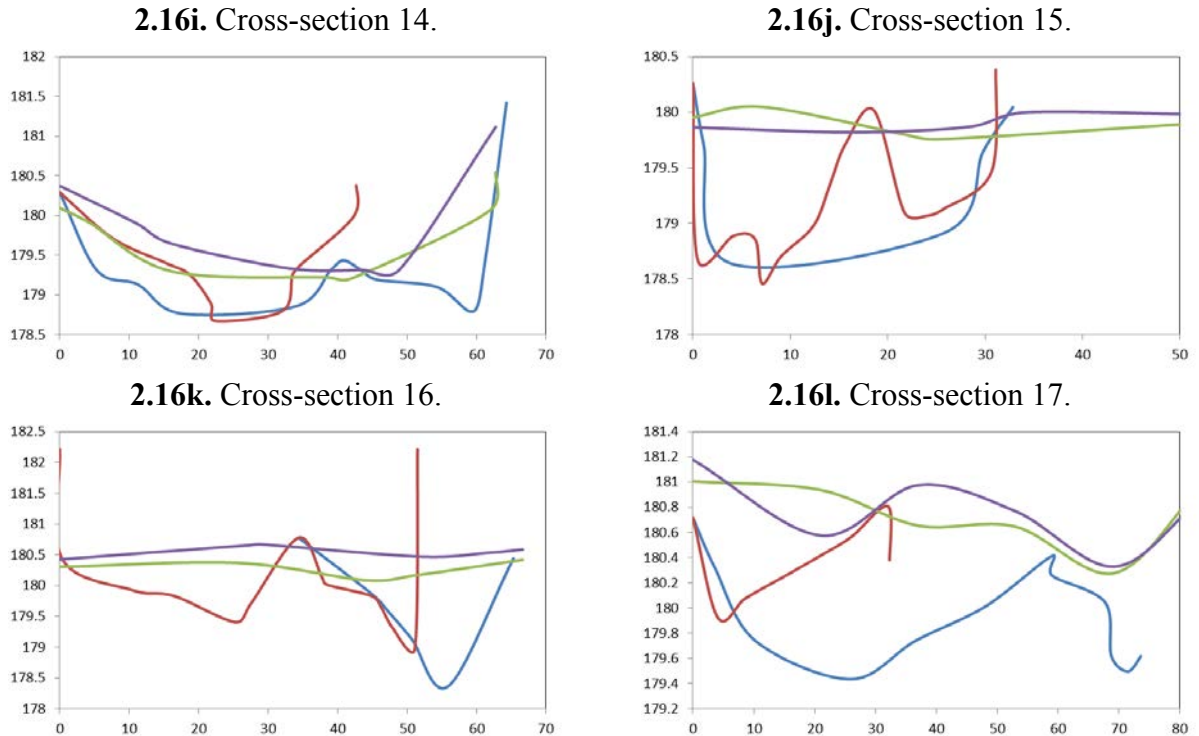
Figure 2.16 (a-l). Comparisons of different cross sections bed elevation using different meshes. Ma2: Mixed meshes; Mb1 Pure quadrilateral mesh.

The Root Mean Square Error (RMSE) for each scenario is listed in Table 2.2.1 Although the RMSE value is as large as 6 ft, Case Mb1 (pure quadrilateral mesh) and Mc1 (Engelund-Hansen Sediment Equation) yielded the best results. It's likely that the pure quadrilateral mesh with Engelund-Hansen's sediment transport equation yields the best match with the measurements.

2.2.5 Computation Efficiency

The computational was performed at a Dell dual-core server. The CPU times are 50 minutes, 5.5 hours and 14 hours, respectively, for M30, M15 and M10 meshes.

Table 2.2.1 Root Mean Square Error for Each Scenario (unit: m)

Case	C6	C7	C8	C9	C10	C11	C12	C13	C14	C15	C16	C17
Ma2	4.885	2.735	2.228	2.127	0.903	0.970	0.162	0.453	0.418	0.922	1.477	0.440
Ma3	6.252	3.041	2.260	2.183	0.866	1.024	0.180	0.303	0.504	0.693	1.753	0.073
Ma4	6.252	3.041	2.260	2.183	0.866	1.024	0.180	0.303	0.504	0.693	1.753	0.082
Mb1	4.875	2.677	2.225	2.225	1.028	0.842	0.084	0.230	0.437	0.433	1.401	0.358
Mc1	4.782	2.781	2.244	2.112	0.913	1.002	0.183	0.436	0.536	0.866	1.689	0.192
Mc2	4.913	2.663	2.241	2.122	0.891	0.988	0.142	0.405	0.462	0.601	1.817	0.361
Mc3	4.792	2.775	2.255	2.108	0.894	0.984	0.174	0.425	0.466	0.771	1.710	0.340
Mc4	4.855	2.713	2.253	2.134	0.867	0.956	0.176	0.451	0.694	0.866	1.597	0.243
Mc5	5.481	2.978	2.255	2.047	0.945	1.028	0.180	0.679	1.299	0.694	1.747	1.481
Mc6	5.481	2.978	2.255	2.047	0.945	1.028	0.180	0.679	1.299	0.694	1.747	1.481
Md1	6.252	3.041	2.260	2.183	0.866	1.024	0.180	0.303	0.504	0.693	1.753	0.142
Md2	6.252	3.041	2.260	2.183	0.866	1.024	0.180	0.303	0.504	0.693	1.753	0.258
Md3	6.252	3.041	2.260	2.183	0.866	1.024	0.180	0.303	0.504	0.693	1.753	0.339
Me1	6.252	3.041	2.260	2.183	0.866	1.024	0.180	0.303	0.504	0.693	1.754	0.266
Me2	6.252	3.041	2.260	2.183	0.866	1.024	0.180	0.303	0.504	0.693	1.753	0.236

2.3 Final Model Run and Results

2.3.1 Computational Grid

The simulation domain is the Lake Mills reservoir reach covering the reservoir delta from Section 3 to Section 17 as shown in Fig.2.2. The simulation boundary including left and right banks is obtained from the boundaries of measured cross sections at April 8th. All other measured data points on the delta from USGS GIS shape files are also used (Fig.2.17a). The bathymetry in the simulated reach is interpolated using the surveyed cross sections and all other measured points on the delta. The measured data points in the tables of USGS report is based on the local coordinates. Conversions are needed to change the elevations to the NAD88 datum. The local elevation was added 0.9 ft to the NGVD29 system, and added 3.625 ft to the NAD88 datum. Therefore, the recorded elevations in the USGS report were added 4.525 ft to the NAD88 datum. The initial bed bathymetry showed two small side channels near both banks (Fig.2.17b). Cross sections, 16 and 17, are used as the inlets. This study used an improved quadrilateral mesh,

shown in Fig.2.18, to accommodate the complex geometry of the delta channels at the beginning of the drawdown experiment.

<div align="center">(a)   (b)</div>
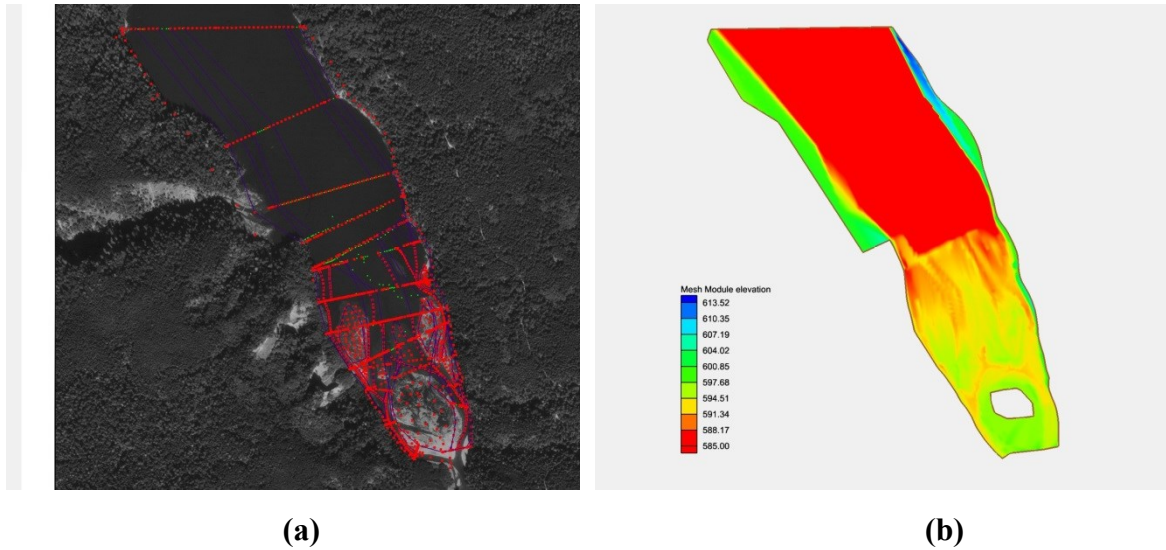
<div align="center">Fig.2.17 Scatter data points and initial bed elevations</div>

<div align="center">Fig.2.18 Quadrilateral computational grid</div>

2.3.2 Simulation Data

Stream flow data were collected at five sites. Daily flows at ELWW, a gaging station that was established just a few weeks prior to the beginning of the drawdown experiment. The stream flow discharge (Fig.2.4) at ELWW gauge is used. The measured discharge is divided into two

parts: one part is 40% of the total discharge at the cross section #16, and the rest is at the cross section #17. Both suspended and bed load sediment discharges measured at ELWW gauge (Fig.2.5) are used as sediment upstream boundary condition.

The lake drawdown began with a full lake at 8:00 am on April 9, 1994. During the experiment, the changes of lake water level were measured and showed in Fig.2.6, which is used as the downstream boundary condition. The particle-size distribution collected at ELD1 station (Fig.2.7) is used for sediment size distribution. The time step for the simulation is 5.0 s. The total simulation time is 360 hours.

2.3.3 Simulation Results

The simulated bed elevations using the new mesh were compared with the measurements on April 23th, and shown in Fig.2.19. Only Yang's equation was used in this calculation in order to compare with the previous results by using only measured cross sections on April 8th, 1994. The final results at Section 3, 4, and 5 showed no erosion or deposition, the same as the measurements. At Section 6, the simulated results underestimated the deposition.   From Section 7 to 11, two large channels are formed at both sides of the delta, while the simulated results also showed two channels formed on the delta, but the channel sizes cannot match the observed ones. The sizes of both channels are smaller than the observed ones. From Section 12 to 15, the simulated results considerably over-estimated the deposition comparing to observed bed elevation.

2.19a. Cross-section 3.　　　　　　　　　**2.19b.** Cross-section 4
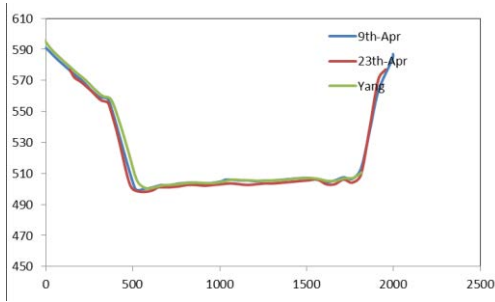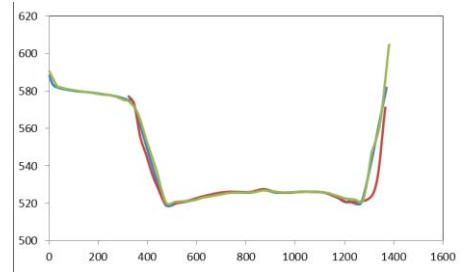
2.19c. Cross-section 5.　　　　　　　　　**2.19d.** Cross-section 6.
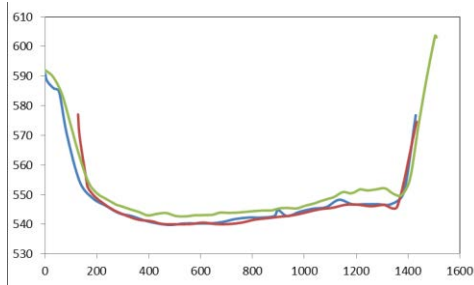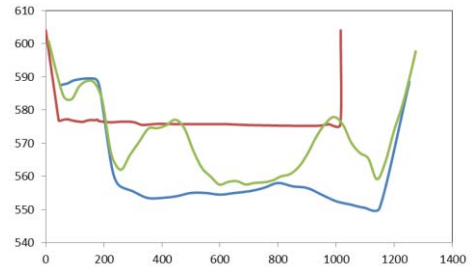
2.19e. Cross-section 7.　　　　　　　　　**2.19f.** Cross-section 8.
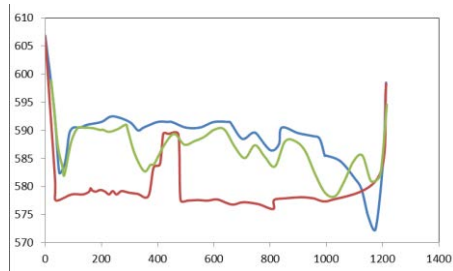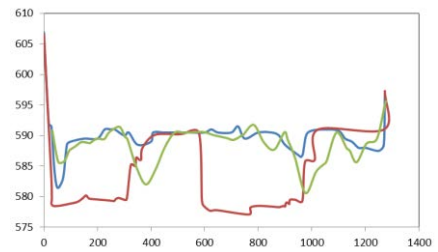
2.19g. Cross-section 9.　　　　　　　　　**2.19h.** Cross-section 10.
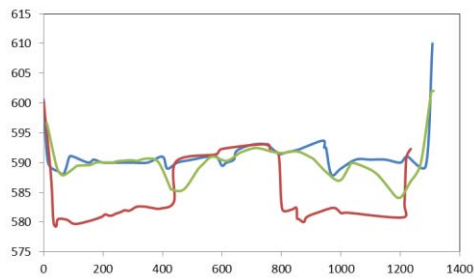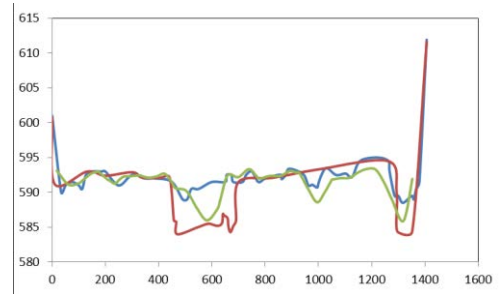
2.19i. Cross-section 11.　　　　　　　　　**2.19j.** Cross-section 12.
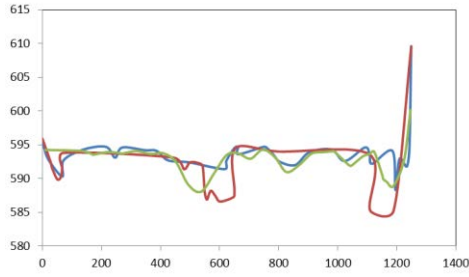
2.19k. Cross-section 13.
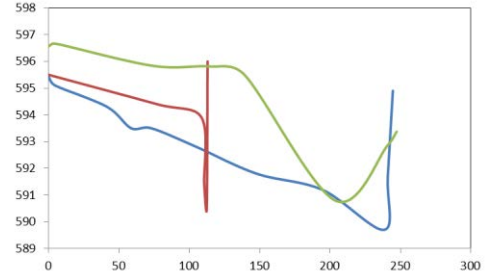
2.19l. Cross-section 14.
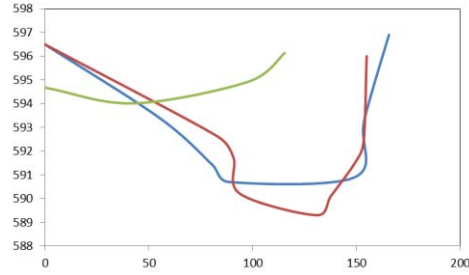
2.19m. Cross-section 15.
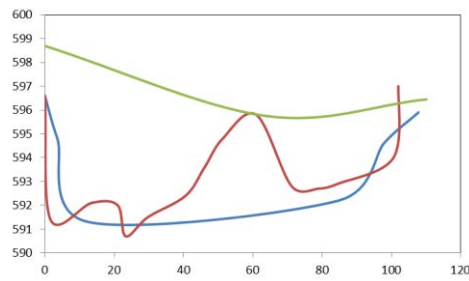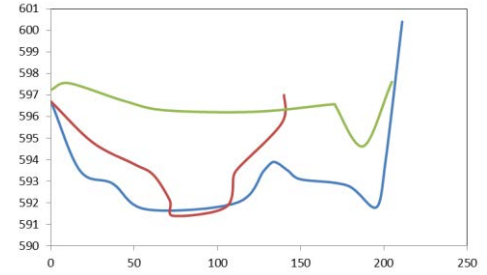
Fig.2.19 Simulated and measured bed elevation changes

The errors of simulated bed elevation changes may due to 1) local turbulence due to woody debris; 2) bank erosion induced channel changes have not been simulated; 3) avulsion or bifurcation processes may also need to be considered.

Part 3: Simulation of Lake Mills Drawdown Experiment Using Delft3D Model

3.1 Introduction

To verify results from SRH2D, the study also simulated the Lake Mill drawdown experiment using the Delft3D model (http://oss.deltares.nl/web/opendelft3d/source-code). Delft3D-FLOW is capable of simulating three dimensional (3D) unsteady incompressible flow and transport phenomena resulting from tidal and/or meteorological forcing. It solves the Reynolds Averaged Navier-Stokes Equations on a structured staggered curvilinear grid using a finite difference scheme (Stelling and van Kester 1994). The governing equations are solved with an Alternating Direction Implicit (ADI) technique (Stelling 1984). Delft3D-FLOW offers two different vertical grid systems σ-grid and Z-grid, and four turbulence closure models: constant eddy viscosity coefficient, algebraic eddy viscosity model, k-L model, and k-ε model.

3.2 Input Data

3.2.1 Computational Grid

The computational grid of the Lake Mills was constructed by using the available geometric and bed elevations data for SRH2D input. This file covers the lake reach from Section 3 to section 17 as shown in Fig.2.2.   The computational grid is a structural grid with M=333, N=60, and K=5 (Fig.3.1a), where M and N are the numbers of grid points on the horizontal plane in the direction of the main flow and normal to the main flow, respectively, and K is the number of layers in the vertical plane. The bathymetry for the entire domain shown in Fig.3.1b was the surveyed data and used the lowest water surface elevation (174.3456m) as the datum. In Fig.3.1b, the bathymetries below the base level are positive while the bathymetries above the base level are negative, which is the Delft3D-FLOW requirement for input data.

| (a) Grid | (b) Bathemetry |
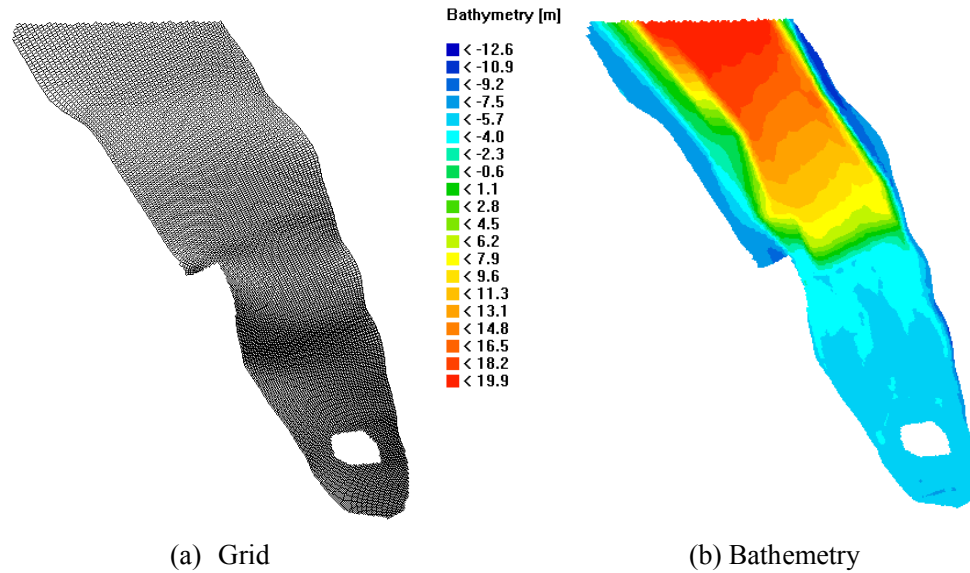
Fig.3.1. Computational grid and bathemetry

3.2.2 Boundary Condition

The drawdown experiment period is from 8:00 am on April 9th to 8:00 am on April 23rd, 1994. The drawdown began with a maximum water surface elevation of 179.832 m and lowered 5.4864 m over one week period from 8:00 am on April 9th to 8:00 am on April 16th. Drawdown rates were about 0.9144 m per day for the first 5 days (April 9th to 14th), 0.6096 m between April 14th and 15th and 0.3048 m between April 15th and 16th. From 8:00 am on April 16th to 8:00 am on April 23rd the water surface elevation was held constant. During the drawdown period, a gaging station ELWW was established upstream from the Lake Mills Delta to provide stream flow discharge and total sediment (suspended plus bedload) discharge. The stream flow discharge (Fig.2.4) in SI units and the total sediment discharge (Fig.2.5) were used as the upstream boundary condition. This recorded lake level was used as the downstream boundary condition (Fig.2.6).

3.2.3 Roughness Coefficient

Constant Manning's roughness coefficient (n) was used for the whole study area. It is found that the simulation is very sensitive to the n-value. For instance, when n-value is in the range 0.03 to 0.15, the simulation diverged. In order to make it converge, the values of n in x and y directions, the horizontal plane, are changed. In this study, the n_x and n_y values are 0.1 and 0.05,

respectively**.**

3.2.4 Sediment Module

The Van Rijn (2000) approach is used to determine the transport of non-cohesive sediment (Delft3D-FLOW user manual).The cohesive sediment module is used in the simulation. In Delft3D-FLOW, the vertical mixing coefficient for sediment is equal to the vertical fluid mixing coefficient calculated by the selected turbulence closure model, i.e.:

$$\varepsilon_s = \varepsilon_f$$

where ε_s is the vertical sediment mixing coefficient for sediment; ε_f is the vertical fluid mixing coefficient calculated by the selected turbulence closure model. In this study, the *k-ε* model is used to determine the coefficient of eddy viscosity. For cohesive sediment fractions, the fluxes between the water and the bed sediment are calculated with the well-known Partheniades-Krone formulations (Partheniades, 1965).

3.3 Results

The simulated bed elevation changes are compared with the measurements on April 23rd as shown in Fig.3.2. In Fig.3.2, the initial bed elevation refers to the bed elevation on April 8th. We noticed that the simulated bed elevation changes for all the sections do not match the measurements. As indicated from the measurements, the study area eroded vertically and horizontally. In this study, only the vertical erosion was simulated, and this is the main reason for the errors in the simulated bed elevation changes.

A PC with Intel Core i7 processor and 4 GB RAM is used for the simulation. The time step of 1 minute is used and the total CPU time is 19643.21 sec.

Cross-section 6

Cross-section 7

Cross-section 8

Cross-section 9

Cross-section 10

Cross-section 11

Cross-section 12
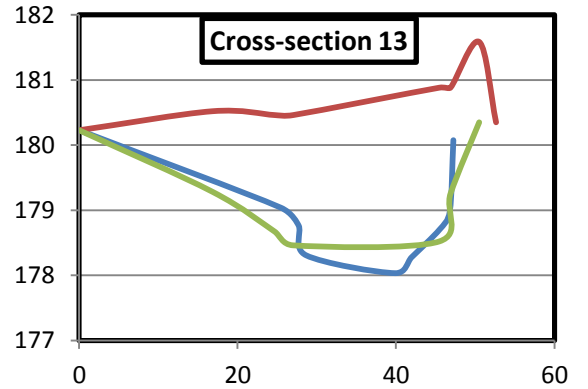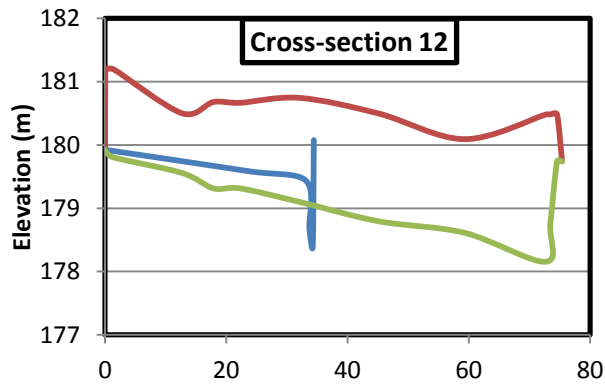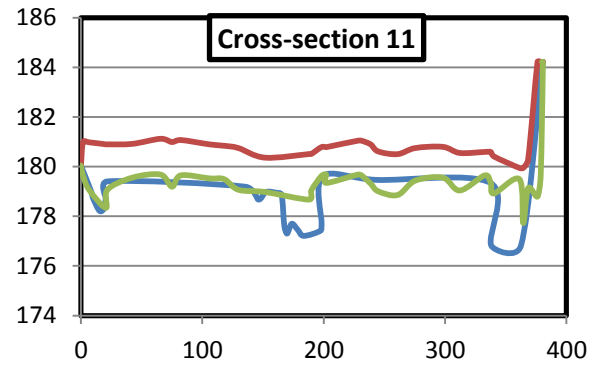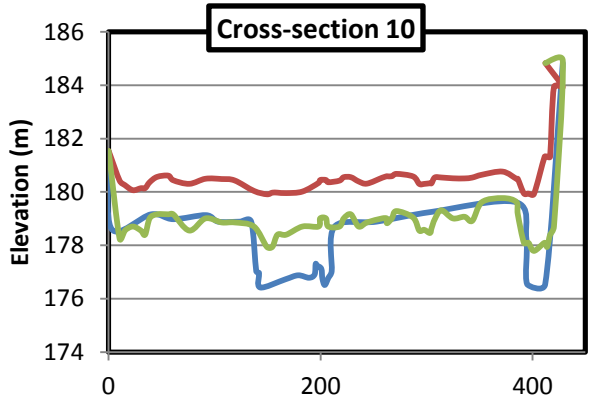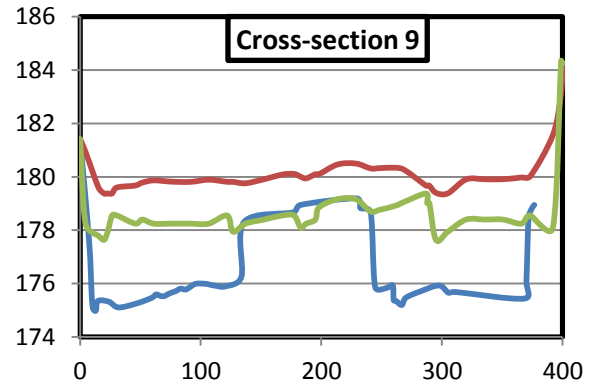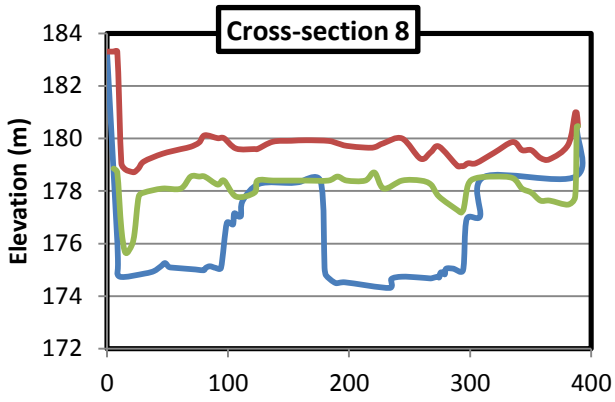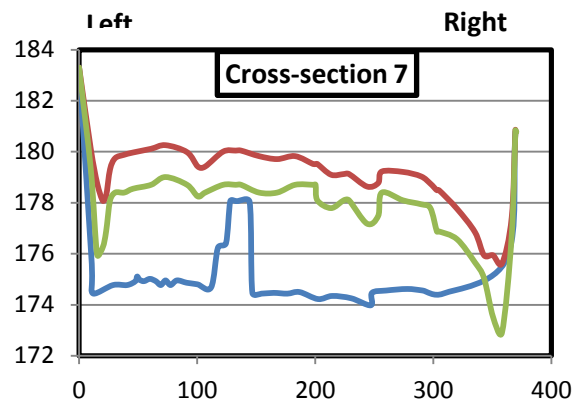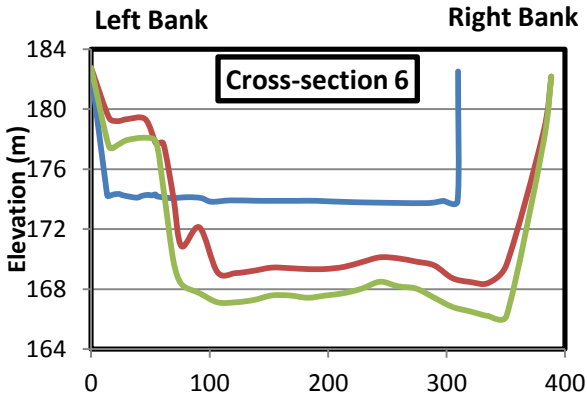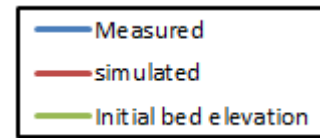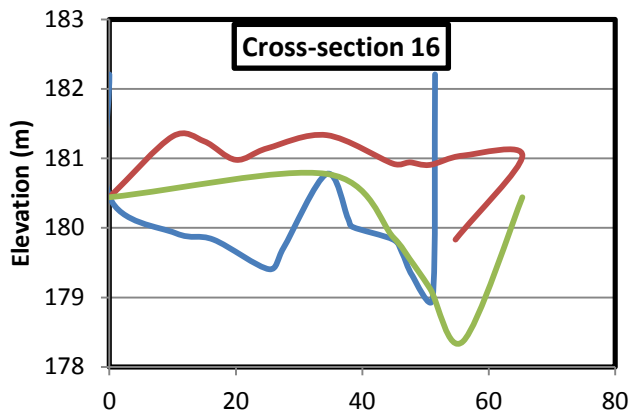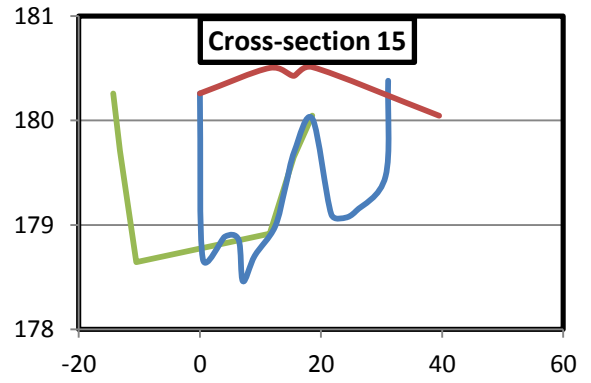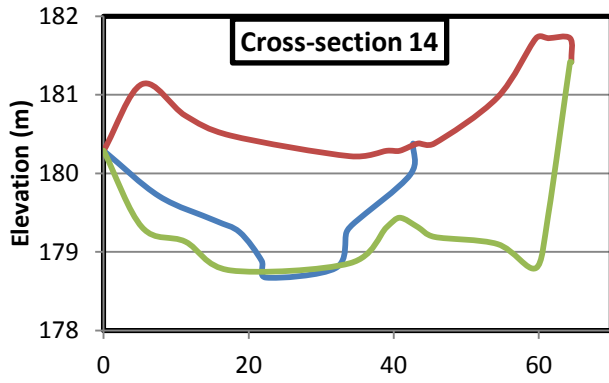
Cross-section 13

Fig.3.2 Simulation results of cross-sections on April 23rd.

Part 4: Conclusion and Recommendation

4.1 Conclusion

This study first applies the SRH2D model to simulate the experimental drawdown of Lake Mills in 1994. The simulated results showed no erosion or deposition within the reservoir at Section 3, 4, and 5, the same as the measurements. At the edge of exposed delta (Section 6), the simulated results underestimated the deposition. From Section 7 to 11 where delta is scoured by the drawdown flow, the simulated results showed two channels formed on the delta, but underestimated erosion occurred in the channels. At the delta upstream (Section 12 to 15), the simulated results considerably over-estimated the deposition comparing to observed bed elevation changes.

To test the sensitivities of modeling results to selected parameters, we chose three different mesh sizes using pure triangular, pure quadrilateral, and mixed triangular and quadrilateral meshes, six different sediment transport equations, three different adaptation lengths, six combinations of roughness coefficients ranging from 0.02-0.06. The results showed that the modeling results are sensitive to sediment equations. Among selected equations, Yang (1973) relation yielded the maximum sedimentation and erosion at sections upstream of the delta, and the results are also sensitive to roughness coefficients. As roughness is increased, more erosion is predicted. However, the maximum roughness value in the simulation reach cannot exceed 0.06 according to field observations. The calibration of roughness coefficients will not lead to accurate results that match the observations. The modeling results are not sensitive to the selection of adaptation length, mesh types, and sizes.

On the other hand, the Delft3D model predicted worse results than those of SRH2D although the exactly same input data were used. Delft3D model predicted deposition rather than erosion for this drawdown experiment except at Section 6. Many reasons may contribute to this result: 1) simulated flow velocity at the upstream of the delta is nearly zero, so no erosion occurred; 2)

Delft3D's sediment transport module is primarily for fine sediment in coastal regions. The approach of cohesive sediment transport needs to be tested for lake drawdown simulation; 3) Delft3D is a quasi-3D model using hydrostatic pressure assumptions, so the turbulence generated erosion cannot be simulated; 4) further calibration of Delft3D model is needed to get better results.

In summary, SRH2D model approximately predicted the erosion in the delta front, in particularly, two side channels formed on the delta. However, the results of SRH2D underestimated the erosion due to water level drawdown that makes the simulated channel erosion much less than the observed. Delft3D model over-estimated deposition, and did not predict the observed erosion.

4.2 Recommendation

As seen from the simulated results, both SRH2D and Delft3D models cannot accurately predicted the observed erosion due to lake level drawdown. As water withdraws from a lake, sediment erosion at channel bottom and bank collapse are visible. The model only predicted very small sediment transport rate due to very small bed shear stresses on the streamwise direction. At present, we cannot tell if the under-predicted bed shear stress is due to the hydrodynamic model because there is no measured flow field that can verify the simulated flow velocity and water surface elevations. Delft3D predicted nearly zero flow velocity on the delta surface where erosion was observed. Whether or not the simulated flow fields, especially shear stress field, from both models are accurate requires further experimental or field data verification. Therefore, we strongly recommend to verify SRH2D and Delft3D using a laboratory experimental case with measured flow field.

Secondly, currently sediment transport equations may not be able to predict sediment transport rate due to water surface drawn down. Water surface is down vertically that will cause

an acceleration of vertical flow. This vertical accelerated flow either directly entrains sediment from bottom or generates drag force that cause sediment transport. The erosion due to the vertical accelerated flow is the major erosion mechanism in lake level drawdown scenario. However, this mechanism was not considered in any sediment transport formula. The sediment transport rate in these two models is determined by the horizontal shear stress, which is a function of depth-averaged horizontal velocity. Therefore, both models under-predict or unable to predict observed erosion.

Therefore, we recommend to verify the flow simulation of SRH2D model using a well-defined laboratory experiment of lake level drawdown. If there is an existing laboratory experiment, it will be ideal. The physical experiment conducted at UM can be a good choice, but needs to check if flow field measurements are available. After the simulated flow field is verified, we recommend modifications to sediment transport equations to account for the effect of vertical accelerated flow on sediment transport.

References

Biron, P. M., Robson, C., Lapointe, M. F., and Gaskin, S. J. (2004b). "Comparing different methods of bed shear stress estimates in simple and complex flow fields." *Earth Surf. Process. Landforms, 29*, 1403-1415.

Biron, P. M., Robson, C., LaPointe, M. F., and Gaskin, S. J. (2005). "Three-dimensional flow dynamics around deflectors." *River Research and Applications*, 21, 961–975.

Childers, D., Kresch, D. L., Gustafson, S. A., Randle, T. J., Melena, J. T., and Cluer, B. (2000). "Hydrologic Data Collected During the 1994 Lake Mills Drawdown Experiment, Elwha River, Washington." USGS, Water-Resources Investigations Report 99-4215.

Delft3D-FLOW User Manual, Version 3.15, Deltares, Rotterdam, The Netherlands.

Dey, S. and Barbhuiya, A. K. (2005). "Flow field at a vertical-wall abutment." *J. Hydraul. Eng.*, 131(12), 1126–1135.

Huthnance, J. M., Humphery, J. D., Knight, P. J., Chatwin, P. G, Thomsen, L., and White, M. (2002). "Near-bed turbulence measurements, stress estimates, and sediment mobility at the continental shelf edge." *Progress in Oceanography*, 52, 17 –194.

Kim, S. C., Friedrichs, C.T., Maa, J. P.-Y., and Wright, L. D. (2000). "Estimating bottom stress in tidal boundary layer from acoustic Doppler velocimeter data." *J. Hydraul. Eng.*, 126(6), 399–406.

McVicar, B. J. and Roy, A. G. (2007). "Hydrodynamics of a forced riffle pool in a gravel bed river: 1. Mean velocity and turbulence intensity." *Water Resour. Res*, 43, W12401, doi10.1029/2006WR005272.

McLelland, S. J. and Nicholas, A. P. (2000). "A new method for evaluating errors in high-frequency ADV measurements." *Hydrol. Process.*, 14, 351–366.

Partheniades, E. (1965)."Erosion and Deposition of Cohesive Soils." Journal of the Hydraulics Division, ASCE 91 (HY 1), 105-139

Pope, N. D., Widdows, J., and Brinsley, M. D. (2006). "Estimation of bed shear stress using turbulent kinetic energy approach – a comparison of annular flume and field data." *Cont. Shelf Res.*, 26, 959–970.

Stelling, G. S. (1984). On the construction of computational methods for shallow water flow problems. *Tech. Rep. 35.*, USGS Professional Paper.

Stelling, G. S., van Kester, J. A. T. M. (1994). On the approximation of horizontal gradients in sigma co-ordinates for bathymetry with steep bottom slopes. *Intern. J. Num. Meth. in Flu.* 18, 915-955

Appendix: Literature Review of Recent Advances in Sediment Transport Model

The conventional sediment transport modeling technique includes 1D, 2D, and 3D hydrodynamic model using the time-averaged sediment transport rate based on excessive bed shear stresses (Duan et al, 2001; Chen and Duan, 2008; Duan and Julien, 2011; Zhang et al., 2013; Apsley and Stansby, 2008; Olsen et al. 2003). The current state-of-the-art sediment modeling technique focuses on the direct simulation of particle transport using the solution of particle momentum equations (Duran et al 2012, Buscombe and Rubin 2012, Tregnaghi et al. 2012; Gabet and Mendoza, 2012). Instantaneous shear stress and the associated particle velocities are experimentally and numerically investigated (Cooper 2012; Tuitz et al. 2012). Three major approaches are summarized in the following sections.

Discrete Element Method (Duran et al. 2012)

The numerical model consists of a discrete element method for particles coupled with a continuum Reynolds averaged description of hydrodynamics. The disadvantages of continuum particle method are: 1) particles motions are assumed parallel to flow direction, the vertical velocity is often neglected; 2) the threshold velocity is not calculated correctly because the interaction between fluid and particles are not accounted for.

The governing equation of particle motion:

$$m\frac{d\vec{u}}{dt} = m\vec{g} + \sum_q \vec{f}^{\,p,q} + \vec{f}^{\,p}_{fluid}$$
$$I\frac{d\vec{\omega}}{dt} = \frac{a}{2}\sum_q \vec{n}^{\,p,q} \times \vec{f}^{\,p,q}$$

(1)

where $\vec{g}$ is the gravitational acceleration, $I = md^2/10$ is the moment of inertia of a sphere, $\vec{f}^{\,p,q}$ is the contact force with grain q, $\vec{n}^{\,p,q}$ is the contact direction, and $\vec{f}^{\,p}_{fluid}$ is hydrodynamic force on grains. The contact forces include 1) normal repulsion, spring-like elastic force; 2)

tangential friction – the tangential displacement between the grains (slides); 3) energy dissipation at the contact is equivalent to a damping force on particles.

Hydrodynamic Force

The hydrodynamic force includes the drag force, the lift force, lubrication force, the corrections to the drag force, and the Archimedes force. If neglecting the lift, lubrication, and correction forces to drag force, then the fluid forces can be written as

$$\vec{f}_{fluid}^{\nu} = \vec{f}_{drag}^{\nu} + \vec{f}_{Arch}^{\nu} \tag{2}$$

The drag force can be expressed as

$$\vec{f}_{drag}^{\nu} = \frac{\pi}{8}\rho_f d^2 C_d(R_u)|\vec{u}-\vec{u}^{-}|(\vec{u}-\vec{u}^{-}) \tag{3}$$

in which $C_d(R_u) = (\sqrt{C_d^\infty} + \sqrt{R_u^c/R_u})^2$ is the drag coefficient in which $R_u = |\vec{u}-\vec{u}^{-}|a/v$, $C_d^\infty = 0.5$ is the drag coefficient of the grain in the turbulent limit ($R_u \rightarrow \infty$) when the drag coefficient becomes a constant.
The Archimedes force;

$$\vec{f}_{Arch}^{\nu} = \frac{\pi}{6}d^3 div\sigma^f \quad \text{in which } \sigma_{ij}^f = -p^f \delta_{ij} + \tau_{ij}^f \tag{4}$$

In the inner region of boundary layer, where most transport takes place, the Archimedes force becomes,

$$\vec{f}_{Arch}^{\nu} = \frac{\pi}{6}d^3(\partial_z \tau_{xz}^f \vec{e}_x - \upsilon_z \rho \ \vec{e}_z) \tag{5}$$

Hydrodynamics

In the presence of particle occupying a volume fraction of ϕ, the hydrodynamics is described by the two-phase flow Reynolds averaged Navier-Stokes equations:

$$\rho_f(1-\phi)D_t u_i = (1-\phi)(-\partial_i p^f + \rho_f g_i + \partial_j \tau_{ij}^f) - F_i \tag{6}$$

where $D_t u_i \equiv \partial_t u_i + u_j \partial_j u_i$ is the inertia force, F_i is the drag force exerted by the grains on the fluid, which can be obtained by averaging the drag force $\vec{f}_{fluid}^{\nu}$ acting on all grains moving around altitude z, in a horizontal layer of area A and thickness dz.

$$\bar{F}(z) = \frac{1}{Adz}\left\langle \sum_{p \in (z:z+dz)} \vec{f}_{drag}^{\nu} \right\rangle \tag{7}$$

The drag force can be calculated as

$$\left\langle \bar{F}_{drag} \right\rangle (z) = \left\langle \sum_{p \in (z:z+dz)} \bar{f}_{drag}^{v} \right\rangle / \sum_{p \in (z:z+dz)} \frac{\pi}{6} d^3 \qquad (8)$$

which is the average drag force acting on grains at a height z per unit grain's volume.

In the inner region of the turbulence boundary layer, both the fluid inertia and the horizontal stress gradients can be neglected, the vertical component of the Reynolds equation becomes:

$$\partial_z p^f = -\rho_f g - \frac{\phi}{1-\phi} \left\langle F_{drag,z} \right\rangle \qquad (9)$$

For steady and homogeneous sediment transport, the contribution of grain's vertical drag to the momentum balance is negligible so that,

$$\partial_z p^f = -\rho_f g \qquad (10)$$

The Archimedes' force becomes

$$\bar{f}_{Arch}^{v} = \frac{1}{6} d^3 (\partial_z \tau^f \bar{e}_x - \rho_f \vec{g}) \qquad (11)$$

Neglecting the inertia and horizontal stresses, the horizontal component of the Reynolds equation becomes

$$\partial_z \tau^f = \frac{\phi}{1-\phi} \left\langle F_{drag,x} \right\rangle \qquad (12)$$

The integration is

$$\tau^f(z) = \rho_f u_*^2 - \int_z^\infty \frac{\phi}{1-\phi} \left\langle F_{drag,x} \right\rangle dz' \qquad (13)$$

The fluid borne shear stress can be approximated using the Prantle-mixing length model,

$$\tau^f = \rho_f (v + l^2 |\partial_z u|) \partial_z u$$
$$\partial_z l = k \left[1 - \exp \left(-\sqrt{\frac{1}{R_c} (\frac{ul}{v})} \right) \right] \qquad (14)$$

Smooth Particle Hydrodynamic Method

Historically, CFD has focused on grid-based method, where two different methods are used: one is Eulerian, and the other is the Lagrangian method (Bozzi and Passoni 2012). Finite element method can be used for Lagrangian method, while finite difference and finite volume methods are dominant for Eulerian method. Both methods need computation grid for the simulation domain. The SPH method is to substitute the grid by a set of arbitrarily distributed nodes, which is more adaptable and versatile than the conventional grid-based methods, especially for those applications with severe discontinuities in the fluid (Gomez-Gesteira et. al.

2010, Groenenboom and Cartwright 2010, Narayanaswamy et al. 2010, Colagrossi et. al. 2010, Hughes and Graham 2010, Rogers et. al. 2010, Khayyer and Gotoh 2010).

SPH is a Lagrangian meshless method in which the fluid domain is represented by a set of irregularly spaced nodal points where physical properties (e.g., mass, density, velocity, position, pressure) are known. Those properties can change with time due to the interaction with neighboring particles. The following integral is the basis:

$$f(\bar{s},t) = \int_v W(\bar{s}-\bar{x},h) f(\bar{x},t) dv \tag{15}$$

where v and dv is the element of volume, $W(\bar{s}-\bar{x},h)$ is the weighting function also called smoothing kernel, h is the size of kernel. The integral is discretized using surrounding particles in the domain:

$$f(\bar{s},t) \approx \sum_j W(\bar{s}-\bar{x}_j,h) f_j(\bar{x}_j,t)\Delta v_j \quad \text{in which} \quad \sum_j W(\bar{s}-\bar{x}_j,h)\Delta v_j = 1 \tag{16}$$

Substituting the volume by $\Delta v_j = m_j / \rho_j$. Eq. 16 becomes

$$f(\bar{s},t) \approx \sum_j \frac{m_j}{\rho_j} W(\bar{s}-\bar{x}_j,h) f_j \tag{17}$$

The most commonly used kernel function is the cubic spline kernel (Monaghan and Kos 1999, Crespo et al., 2007, Crespo et al. 2008). In general, the accuracy of the SPH interpolation increases with the order of the polynomial used in the weighting function (Crepo et al. 2007). The kernel functions in Monaghan et al. (1999) is

$$\begin{cases} W(r,h) = \dfrac{10}{7\pi h^2}(1-\dfrac{3}{2}q^2+\dfrac{3}{4}q^3) & q<1 \\[2mm] W(r,h) = \dfrac{10}{28\pi h^2}(2-q)^3 & 1<q<2 \\[2mm] W(r,h) = 0 & q>2 \end{cases} \tag{18}$$

in which *r*= distance between particles, *h*=smoothing length, and *q=r/h*.

One of the main advantages of SPH is that a differential interpolation of any function can be

57

constructed from its values at the particles simple by using a differentiable kernel in the summation processes. For a scalar function A, its gradient can be calculated as

$$\nabla A_i(\bar{s},t) = \sum_j \frac{1}{\rho_j} \nabla W (\bar{s} - \bar{x}_j, n) A_j$$

using $\rho \nabla A = \nabla(\rho A) - A \nabla \rho$ (19)

$$\nabla A_i(\bar{s},t) = \sum_j \frac{1}{\rho_j}(A_j - A_i) \nabla W (\bar{s} - \bar{x}_j, n)$$

Similarly, the divergence can be calculated as

$$div(\bar{u}_i) = \sum_j \frac{1}{\rho_j}(\bar{u}_j - \bar{u}_i) \nabla W (\bar{s} - \bar{x}_j, n)$$ (20)

The SPH discrete summation procedure can generate important inaccuracies in the vicinity of the boundaries and close to the free-surface where the normalization condition is not fulfilled.to overcome this problem, corrections to kernel and/or the 1st derivative, or performing density filter are proposed. For example, the zeroth-order Shepard density filter can be applied every 20-50 time steps;

$$\rho_i^{new} = \sum_j \rho_j \tilde{W}_{ij} \frac{m_j}{\rho_j} \qquad \sum_j W_{ij}$$ (21)

where the kernel can be corrected using a zeroth-order correction:

$$\tilde{W}_{ij} \qquad \frac{W_{ij}}{\sum_j W_{ij} \frac{m_j}{\rho_j}}$$ (22)

Another simple kernel and kernel gradient correction is developed by Chen et al. (1999). In 1D, the corrected kernel approximation for a variable f_i (e.g., the velocity) is

$$f_i = \frac{\sum_j \frac{m_j}{\rho_j} f_j W_{ij}}{\sum_j \frac{m_j}{\rho_j} W_{ij}}$$ (23)

The corrective estimate of the 1st order derivative becomes:

$$A_i \nabla f_i = F_i$$

$$\text{where } A_i = \sum_j \frac{m_j}{\rho_j}(x_j - x_i)\nabla_i W_{ij} \quad F_i = \sum_j \frac{m_j}{\rho_j}(f_j - f_i)\nabla_i W_{ij} \tag{24}$$

This method applied to both vector and scalar.

Application to Flow and Sediment Transport Simulation

The conservation law for a compressible fluid can be written as

$$\frac{\partial \rho}{\partial t} + div(\rho \vec{u}) = 0 \quad \text{(Eulerian form)}$$

$$\frac{1}{\rho}\frac{\partial \rho}{\partial t} + div(\vec{u}) = 0 \quad \text{(Lagrangian form)} \tag{25}$$

The discretized form is

$$\left(\frac{d\rho}{dt}\right)_i = \rho_i \sum_j \frac{m_j}{\rho_j}(\vec{u}_i - \vec{u}_j) \cdot \nabla_i W_{ij} \tag{26}$$

For steady flow, a simple interpolant is

$$\rho_i = \sum_j m_j \nabla_i W_{ij} \tag{27}$$

The conservation of momentum in its Lagrangian form becomes

$$\frac{d\vec{u}}{dt} = -\frac{1}{\rho}\nabla p - \vec{g} \tag{28}$$

The discretized form for particle i becomes;

$$\frac{d\vec{u}}{dt} = -\sum_j m_j\left(\frac{p_j}{\rho_j^2} + \frac{p_i}{\rho_i^2}\right)\nabla_i W_{ij} - \vec{g} \tag{29}$$

Including the laminar viscosity and sub-particle scale (SPS) turbulence, the momentum conservation equations becomes,

$$\frac{d\vec{u}}{dt} = -\frac{1}{\rho}\nabla p - \vec{g} + \nu_0 \nabla^2 \vec{u} + \frac{1}{\rho}\nabla \cdot \tilde{\tau} \tag{30}$$

The laminar viscosity term can be discretized as

$$\nu_0 \nabla^2 \vec{u} = \sum_j m_j \left[\frac{4\nu_0 \vec{x}_{ij} \nabla_i W_{ij}}{(\rho_i + \rho_j)(r_{ij}^2 + \eta^2)}\right]\vec{u}_{ij} \tag{31}$$

in which $\vec{x}_{ij} = \vec{x}_i - \vec{x}_j, \eta^2 = 0.01h^2$.

The stress tensor in SPS model is

$$\tilde{\tau}_{\mu\nu} \ldots \tau_t \tilde{L}_{\mu\mu} \quad \frac{2}{3} \tilde{\tau}_{kk} \tilde{\tau}_{\mu\nu} \quad \frac{2}{3} C_l \Delta l^2 \delta_{\mu\nu}) \tag{32}$$

In which Δl is particle-particle spacing, $C_l = 0.0066$, the Favre-filtered rate of strain tensor is

$$\tilde{L}_{\mu\nu} \quad \frac{1}{2}\left(\frac{\partial \tilde{u}_\nu}{\partial x_\nu} \quad \frac{\partial}{\partial x_\mu}\right) \ldots \tau_t \quad [\ldots (C_s \ldots) \tilde{\tau}] \tag{33}$$

in which $C_s = 0.12$ the Samgorinsky constant and the local strain rate $|\tilde{L}| \quad (\ldots_{\mu\nu} \tilde{S}_{\mu\nu})^{1/2}$. The discretized form becomes:

$$\frac{1}{\rho_i}\left(\frac{\partial \tilde{\tau}_{\mu\nu}}{\partial x_\nu}\right)_i = \sum_j m_j \left(\frac{\tilde{\tau}_{\mu\nu,j}}{\rho_j^2} + \frac{\tilde{\tau}_{\mu\nu,i}}{\rho_i^2}\right) \frac{\partial}{\partial x_\nu} \tag{34}$$

The equation of state can be used to solve for the pressure of weakly compressible flow:

$$p = B\left[\left(\frac{\rho}{\rho_0}\right)^\gamma - 1\right] \tag{35}$$

in which $B = c_0^2 \rho_0 / \gamma$, $c_0 =$ speed of sound at the reference density $\rho_0 = 1000 kg/m^3$, γ is a constant between 1 and 7 (7 is for ocean application).

The sediment particle motion equation is written as

$$m_s \frac{d\bar{u}_s}{dt} = \sum \vec{F}_i \tag{36}$$

in which m_s is the mass of sediment particle, $\bar{u}_s$ is the velocity vector of sediment particle, and $\vec{F}_s$ is the forces on sediment particles including drag force, bouyancy force, and added mass. The constant drag force can be written as

$$F_D = \frac{1}{2} \rho_f C_D A |u_f - u_s| (u_f - u_s) \tag{37}$$

in which $C_D =$ drag coefficient, A= frontal area of sediment particle, u_f and u_s are fluid and particle velocities, respectively. The sediment transport equation can be solved similarly to flow particle.

References

Apsley D. David, Stansby, K. Peter (2008). Bed-load sediment transport on large slopes: model formulation and implementation within a RANS solver, *J. of Hydraulic Engrg.*, Vol.134, No.10, doi:10.1061(ASCE)0733-9429(2008)134:10(1440).

Bozzi, S. and Passoni, G. (2102) Mathematical modelling of bottom evolution by particle deposition and re-suspension, *Applied Mathematical Modelling*, 36, 4186-4196.doi: 10.1016/j.apm.2011.11.048.

Buscombe, D. and Rubin, D., M., (2012) Advances in the simulation and automated measurement of well-sorted granular material, *J. of Geophysical Research*, 117, F02001, doi:10.1029/2011JF001974.

Chen, D., and Duan, J. G. (2008). "Case study: two-dimensional model simulation of channel migration processes in West Jordan River, Utah." *J. Hydraul. Eng.*, 134(3), 315-327.

Chen, J.K., Beraun, J.E., Carney, T.C. (1999(. A corrective Smoothed Particle Method for boundary value problems in heat conduction. *Comput. Meth. Appl. Mech. Engrg.* 46, 231-252.

Colagrossi, A., Colicchio, G., and Lugni, C. (2010). A study of violent sloshing wave impacts using an improved SPH method, *J. Hydraul. Res.*, Vol. 48, Special Issue: SI, 94-104.

Crespo, A.J.C., Gomez-Gesteira, M., Dalrymple, R.A. (2007). 3D SPH Simulation of large waves mitigation with a dike. *J. Hydr. Res.* 45(5), 631-642.

Crespo, A.J.C., Gomez-Gesteira, M., Dalrynple, R.A. (2008). Modeling dam break behavior over a wet bed by a SPH technique. *J. Wtrwy. Port, Coastal and Ocean Engrg.* 134(6), 313-320. Doi:10.1061/(ASCE)0733-950X(2008) 134:6(313).

Cooper, J. R. (2012) Does flow variance affect bedload flux when the bed is dominated by grain roughness? *Geomorphology*, 141-142, 160-169. Doi:10.1016/j.geomorph.2011.12.039.

Duan, J. G., Wang, S.S.Y., and Jia, Y. F. (2001). "The applications of the enhanced CCHE2D model to study the alluvial channel migration processes." J. Hydraul. Res., 39(5), 469-480.

Duan, J. G., and Julien, P. Y. (2010). "Numerical simulation of meandering evolution." J. Hydrol., 391, 34-46, doi:10.1016/j.jhydrol.2010.07.005.

Duran, O., Andreotti, B., Claudin, P. (2012) Numerical simulation of turbulent sediment

transport from bed load to saltation, *Physics of Fluids*, 24, 103306,doi:10.1063/1.4757662.

Gabet, E. J., Mendoza, M.K. (2012) Particle transport over rough hillslope surfaces by dry ravel: experiments and simulations with implications for nonlocal sediment flux, *Journal of Geophysical Research*, Vol. 117, F01019, doi:10.1029/2011JF002229.

Gomez-Gesteira, M.; Rogers, B. D.; Dalrymple, R.A. (2010) State-of-the-art of classical SPH for free-surface flows, *J. Hydraul. Res.*, Vol. 48, Special Issue: SI, 6-27.

Groenenboom, P. H. L.; Cartwright, B. K. (2010) Hydrodynamics and fluid-structure interaction by coupled SPH-FE method, *J. Hydraul. Res.*, Vol: 48 Special Issue: SI, 61-73.

Hughes, J. P., Graham, D. I. (2010). Comparison of incompressible and weakly-compressible SPH models for free-surface water flows, *J. Hydraul. Res*., Vol. 48, Special Issue: SI, 105-117.

Khayyer, A., Gotoh, H. (2010). On particle-based simulation of a dam break over a wet bed, *J. Hydraul. Res*., Vol. 48, No 2, 238-249.

Monaghan, J.J., Cas, R.A.F., Kos, A.M., Hallworth, M. (1999). Gravity currents descending a ramp in a stratified tank. *J. Fluid Mech*. 379, 39-70.

Monaghan, J.J., Kos, A. (1999). Solitary waves on a Cretan beach. J. Wtrwy. Port, Coastal Engrg. 125(3), 145-154.

Narayanaswamy, M.; Cabrera C., Alejandro J.; Gomez-Gesteira, M. (2010). SPHysics-FUNWAVE hybrid model for coastal wave propagation *J. Hydraul. Res*., Vol. 48, Special Issue: SI, 85-93.

Olsen, N.R.B., (2003). Three Dimesnional CFD Modeling of Self-Forming Meandering Channel, *J. of Hydraul. Engrg.,* Vol 129, No.5, 366-372.

Rogers, B. D., Dalrymple, R. A., Stansby, P. K. (2010). Simulation of caisson breakwater movement using 2-D SPH, *J. Hydraul. Res*., Vol. 48, Special Issue: SI, 135-141.

Tregnaghi M., Bottacin-Busolin, A., Tait, S., Marion, A., (2012) Stochastic determination of entrainment risk in uniformly sized sediment beds at low transport stages: 2. Experiments,

Journal of Geophysical Research, Vol. 117, F04005, doi:10.1029/2011JF002135.

Tuitz C., Exner, U. Preh, A., and Grasemann, B. (2012) The influence of particle orientation on the loading condition of pebbles in fluvial gravel, *Granular Matter*, 14:639-649. DOI 10.1007/s10035-012-0365-9.

Zhang, S., Duan, J. G., and Strelkoff, T. S. (2013) "Gain-scale non-equilibrium sediment transport model for unsteady flow." Journal of Hydraulic Engineering, 139(1), 22-36.